13 Self Interaction Corrections to Density Functional Theory

Mark R. Pederson
Department of Physics
The University of Texas at El Paso
500 W University Avenue, El Paso, TX 79968, USA

Contents

E. Pavarini and E. Koch (eds.)
Orbital Physics in Correlated Matter
Modeling and Simulation Vol. 13
Forschungszentrum Jülich, 2023, ISBN 978-3-95806-689-2
http://www.cond-mat.de/events/correl23

1 Motivation

Since the earliest days of quantum mechanics researchers have philosophized about the physical meaning of electronic wavefunctions and have often sought to find rigorous means for interpreting both localized and canonical representations of the electronic degrees of freedom and for building more effective or efficient theories based upon localized orbitals [1–27]. Two of the earliest papers by Pauling and Koopmans highlight the dichotomy of viewpoints. Pauling [1] pointed out that localized sp^3 orbitals helped to explain energy differences between separated and condensed phases while Koopmans [2] showed that it was in fact canonical orbitals that best explained energy differences involving removal or addition of electrons. The discussion continues today with reasons, both conceptual and rigorous, for thinking in terms of both pictures. And the overlapping discussion spans all fields of quantum-mechanical inquiry especially in cases where computational constraints require consideration of quantum-mechanical formulations that are not unitarily invariant within their representation. Here these problems are discussed within the self-interaction correction to density functional theory and one aspect of this discussion partially unifies early work of Pauling [1], Wannier [3], Löwdin [4] and Edmiston, and Ruedenberg [5].
Before introducing the Fermi-Löwdin-Orbital formulation and discussing it within the framework of the self-interaction correction (SIC) to density-functional approximations (DFA), we motivate the use of the Fermi orbital with five questions, all of which have the same answer:

1. Can the concept of Wannier functions in condensed-matter physics [3], sp^n hybridized orbitals in atomic physics, localized molecular orbitals in molecular physics [4, 5] be formulated within a universal formulation?

2. Is there a means to generalize the concept of Wannier functions, which are currently only defined in insulating systems, to metallic systems?

3. Is there a way to create a unitary transformation, generally thought of as a discrete operator represented as an $N \times N$ matrix, that explicitly depends continuously on the one-particle density matrix?

4. Is there a way to start with a set of Kohn-Sham orbitals and define a quasi-classical "electronic geometry" that is, in some way, the reciprocal lattice of the Kohn-Sham orbitals?

5. How does one re-formulate the self-interaction correction [8] to the density-functional approximation in a manner that assures the resulting energy is both size consistent and unitarily invariant?

The answer to all of the above questions is that there is indeed a common construction, now commonly referred to as Fermi-Löwdin orbitals [19, 20] that are indeed the answer to all of the above questions. In the early 1980's Luken and coworkers [10], due to their interest in electron diffusion, considered the use of the so-called Fermi-exchange hole, $\rho(r, r')/\sqrt{\rho(r)}$, to define a set of orthonormal orbitals that sum to the total density of an electronic system. In

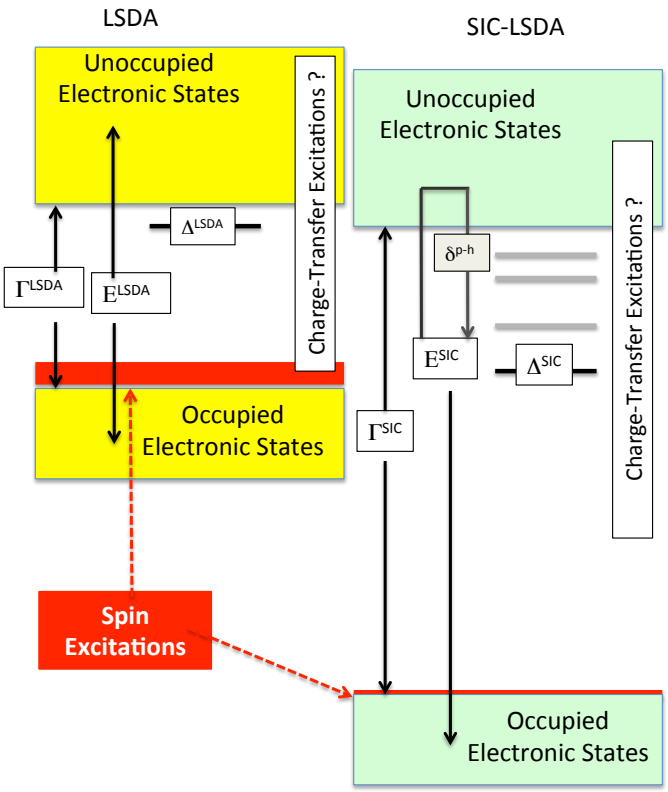

Fig. 1: *Qualitative comparison of electronic structures and excitations as approximated by the local-spin-density approximation and the self-interaction-corrected approximations to density functional theory: The HOMO/LUMO/Band gaps (Γ) increase. The location of the defect levels (δ) are moved away from the conduction band. The spin excitation spectrum narrows.*

the following, we discuss how such orbitals address one of the greatest challenges to the field of density-functional theory. In this chapter I try to compare and contrast the earliest versions of the self-interaction corrected density functional [8] with a new formalism referred to as the Fermi-Löwdin Self-Interaction Correction. The work discussed here was originally discussed as parts of Ref. [9,11,19–21,25,27] and involved collaborations with many authors who I thank and refer to here and in the acknowledgments. I have attempted to discuss the work in the most sensible way based on today's knowledge rather than on the chronological development.

SIC-induced improvements of spectroscopies

The qualitative differences between DFA and SIC-DFA are depicted in Fig. 1. The SIC pulls down the occupied states relative to the unoccupied states which generally leads to a gap (Γ) that is improved in comparison to experiment. Localized excitations in a vacuum or excitons in a wide-gap insulator (depicted as E) can be difficult to identify within LSDA calculations as they often appear above the conduction band. In DFA-SIC, with an approximation to the particle-hole interaction (δ), the description of such excitations can be improved. For defects in solids, where localized levels occupy the gap, LSDA and GGA calculations tend to place the defect levels (labeled by Δ) too close to, or overlapping, with the unoccupied conduction band. However, SIC-LSDA pulls the defect levels down and generally predicts shallow lev-

els in a qualitatively correct location relative to the conduction level. With inclusion of SIC and a particle-hole interaction, an unoccupied continuum of defect levels, expected from the Mott-Gurney theorem, begins to emerge. Consensus is emerging in regard to the differences between SIC and DFA charge-transfer excitations. Examples suggest that DFA can dramatically underestimate these energies and that an approximate self-interaction-corrected energy with a particle-hole interaction restores the correct asymptotic form for donor-acceptor and other charge-transfer excitations. For example, in a vacuum, these energies are found to be close to $I-A-1/R$, where I is the donor ionization energy, A is the acceptor electron affinity and R is the separation between the particle and hole. For spin excitations, determined from DFA-based derivations of Heisenberg Hamiltonians, a large number of calculations show that the spin-excitation energies are overestimated due to DFA's tendency to slightly delocalize the d-electrons, since the kinetic exchange interactions increase exponentially as the d-electrons delocalize. Therefore inclusion or partial inclusion of self-interaction corrections lowers the spin-excitation energies and improves agreement with experiment. While not depicted in the picture, vibrational spectra seem to be relatively well accounted for within DFA. However, since polarizabilities are dependent on SIC, the Raman intensities are also expected to show some dependence on the inclusion of self-interaction corrections. Original efforts and motivations within SIC sought to improve gaps and excitations through the use of eigenvalues. As alluded to at the very beginning of this chapter, there are conditions for which eigenvalues provide rigorous estimates for electronic processes but not for all possible changes in orbital rearrangements. While a generalized Koopmans' theorem is a good goal, changes in computational speed and the need for unambiguous accuracy will definitely favor total energy difference calculations rather than uses of Koopmans-like pictures for all possible excitations. One of the ways that the dialogue and interpretations about self-interaction-corrected and standard DFA eigenvalue differences needs to change is that when there are qualitative differences it often means that delta-SCF calculations are not possible within DFA but are within SIC. That is, a qualitatively correct electronic structure within SIC allows for total energy differences but a qualitatively incorrect DFT electronic structure does not.

In 1981 Perdew and Zunger formulated the self-interaction correction to ensure that any approximation to the density-functional would be correct in the one-electron limit. This was accomplished by modifying any approximation to the universal density-functional, $E_{xc}^{DFA} \equiv [n_\uparrow, n_\downarrow]$, according to

$$E_{xc}^{DFA} \rightarrow E_{xc}^{SIC\text{-}DFA} = E_{xc}^{DFA} - \sum_{i,\sigma} \left(U[\rho_{i,\sigma}] + E_{xc}^{approx}[\rho_{i,\sigma}, 0] \right). \tag{1}$$

In the above equation, the SIC (localized) orbitals $\{\varphi_{i\sigma}\}$ are used to define orbital densities according to: $\rho_{i\sigma}(\boldsymbol{r}) = |\varphi_{i\sigma}(\boldsymbol{r})|^2$. The terms $U[\rho_{i,\sigma}]$ and $E_{xc}^{approx}[\rho_{i,\sigma}, 0]$ are the exact self-Coulomb and approximate self-exchange-correlation energies, respectively. In the original formulation by Perdew and Zunger, the density-functional was approximated in terms of spin densities only but the formulation is not constrained by such an assumption. Modern-day approximations to the exchange-correlation energy generally include gradients of the spin densities which would then require corresponding gradients of orbital densities.

In reference to the work discussed in this section, the original PZ formulation led to a definition for the energy functional that did not transform like the density and posited that atomic-like orbitals might be the most appropriate set of orbitals for defining the SIC. This idea was formalized between 1981–1986 through the concept of localized and canonical orbitals in orbital-dependent density functional theory. It was demonstrated that, within the constraint that the orbitals used for constructing the SIC were orthonormal and constructed from a unitary transformation on the occupied orbital space, that the orbitals which minimize the self-interaction corrected functional satisfy the following equations [9]

$$\left(H_o + V_i^{SIC}\right)|\varphi_i\rangle = \sum_j \lambda_{ji}\,|\varphi_j\rangle \quad \text{and} \quad \left\langle\varphi_{i\sigma}\right| V_{i\sigma}^{SIC} - V_{j\sigma}^{SIC}\left|\varphi_{j\sigma}\right\rangle = 0, \tag{2}$$

with $V_{i\sigma}^{SIC}$ the partial functional derivative of Eq. (1) with respect to the orbital density $n_{i\sigma}$. A Jacobi-like approach for solution of the "localization equations" was shown to work well [9,11] and it was determined that in analogy to Koopmans' theorem in Hartree Fock, the eigenvalues of the Hermitian Lagrange multiplier matrix were expected to be in good agreement with experimental electron removal energies [11]. The localized orbitals obtained from these equations were found to be topologically similar to sp^3 hybrids in atoms, alternative energy-localized orbitals in molecules, and Wannier functions in insulating solids. While this formulation offered some advantages over density-functional approximations it was still not explicitly formulated as an energy that was dependent only on the density matrix. As a result this version of the self-interaction correction was neither unitarily invariant nor size consistent.

2 Introduction to Fermi-Löwdin orbitals and preliminary applications

The orbitals introduced here, for the purpose of implementation of the self-interaction correction, have been proposed by Luken *et al.* in the early 1980s and more recently (since 2014) considered for improving density-functional approximations. Within the group of scientists interested in the self-interaction error to density-functional theory they are now commonly referred to as Fermi-Löwdin orbitals because they are based on the concept of the exchange hole in Hartree-Fock, often referred to as the Fermi-exchange hole, and because their construction relies upon a technique known as Löwdin's method of symmetric orthormalization. To further motivate the derivation of the Fermi-Löwdin orbitals let us algebraically manipulate the expression for the exact exchange energy for spin σ as

$$\begin{aligned} E_\sigma^x &= -\frac{1}{2}\int d\vec{a}\int d\vec{r}\,\frac{\left|\sum_\alpha \psi_{\alpha\sigma}^*(\vec{r})\psi_{\alpha\sigma}(\vec{a})\right|^2}{|\vec{r}-\vec{a}|} = -\frac{1}{2}\int d\vec{a}\,\rho_\sigma(\vec{a})\int d\vec{r}\,\frac{\left|\sum_\alpha \psi_{\alpha\sigma}^*(\vec{r})\psi_{\alpha\sigma}(\vec{a})\right|^2}{\rho_\sigma(\vec{a})\,|\vec{r}-\vec{a}|} \\ &= -\frac{1}{2}\int d\vec{a}\,\rho_\sigma(\vec{a})\int d\vec{r}\left[\frac{\rho_\sigma(\vec{r},\vec{a})}{\sqrt{\rho_\sigma(\vec{a})}}\right]\left[\frac{\rho_\sigma(\vec{a},\vec{r})}{\sqrt{\rho_\sigma(\vec{a})}}\right]\frac{1}{|\vec{r}-\vec{a}|} \\ &= -\frac{1}{2}\int d\vec{a}\,\rho_\sigma(\vec{a})\int d\vec{r}\,\frac{\left|F_{\vec{a}\sigma}(\vec{r})\right|^2}{|\vec{r}-\vec{a}|} \end{aligned} \tag{3}$$

with the Fermi-orbital, defined as $F_{\vec{a}\sigma}(\vec{r}) \equiv \rho_\sigma(\vec{r},\vec{a})/\sqrt{\rho_\sigma(\vec{a})}$. In the above equation, the exact exchange energy has first been expressed in terms of the single-particle density matrix, $\rho_\sigma(\vec{r},\vec{a}) = \sum_\alpha \psi^*_{\alpha\sigma}(\vec{r})\,\psi_{\alpha\sigma}(\vec{a})$ and then the expression within the double integral has been multiplied and divided density $\rho_\sigma(\vec{a}) = \rho_\sigma(\vec{a},\vec{a})$. Examination of the expression shows that the Fermi-Exchange hole, evaluated at any point in space, $\vec{a}$, integrates to unity and that one can think about the exchange energy density as the interaction of the total density $\rho_\sigma(\vec{a})$ interacting with the Fermi-Exchange-hole density $F_{\vec{a}\sigma}(\vec{r})$ that is redefined at each point, $\vec{a}$.
Because the Fermi-Exchange-Hole transforms like the density under unitary transformations any quantity that depends on the Fermi-Exchange-Hole is also unitarily invariant. As such, the following reformulation of the Perdew-Zunger self-interaction was developed in terms of the spin-density-matrix and N electronic positions according to the following prescription:

1. For a trial set of Kohn-Sham (KS) orbitals $\{\psi_{\alpha\sigma}\}$ find a special set of N_σ positions in space $\{\boldsymbol{a}_{1\sigma}, \boldsymbol{a}_{2\sigma}, \ldots, \boldsymbol{a}_{N_\sigma\sigma}\}$ which provide a set of N_σ normalized linearly independent, but not orthogonal Fermi-orbitals $\{F_{1\sigma}, F_{2\sigma}, \ldots, F_{N_\sigma\sigma}\}$. By their construction from the density matrix, these Fermi-orbitals will always lie in the space spanned by the KS orbitals but are not guaranteed to span that space (For example if one defines each Fermi-orbital in terms of the same position the N Fermi-orbitals would be identical. These positions are now called Fermi-Orbital Descriptors (FODs).

2. When a set of N FODs, that provide a set of Fermi-orbitals that span the space of the Kohn-Sham orbitals is found, use Löwdin's method of symmetric orthonormalization to transform the set of FOs to a set of localized orthonormal orbitals $\{\varphi_{1\sigma}, \varphi_{2\sigma}, \ldots, \varphi_{N_\sigma\sigma}\}$ that are a unitary transformation on the KS orbitals. The resulting Fermi-Löwdin orbitals (FLOs) depend upon the set of FODs which means that the self-interaction energy also depends on the FODs.

3. Minimize the energy as a function of the KS orbitals and the set of FODs. The minimization with respect to the FODs can be performed using methods that are commonly used to optimize molecular geometries.

In this section some simple applications of this FLOSIC methodology are presented. The goal is to introduce both real and (briefly) complex SIC orbitals and compare them within the context of the original version of self-interaction corrections and the FLOSIC version of self-interaction corrections. By considering simple atoms, the N_2 molecule, and a cubic Brillouin zone with uniform density the reader should gain an understanding that complex Kohn-Sham orbitals do not require complex FODs or complex local orbitals, that there are times when symmetry considerations or energy considerations argue for the use of complex orbitals, and there are times when bond-breaking-considerations argue for FLOs that break spin symmetry. Appreciating these issues early on will help prepare practitioners for future improvements in the theory and implementation of the FLOSIC formulation. However the reader will also be prepared for the discussions about complex FLOs that appears later in this chapter.

2.1 Closed shell atoms

As a way of introducing Fermi-Löwdin orbitals and the Fermi-orbital-descriptors that define them and as a way of attempting to encourage universality across disciplines we can start by thinking about the $2sp^3$-hybrids. This also provides a simple analytical example that can be based upon the hydrogenic orbitals. For principal quantum numbers $n = 2$, the hydrogenic orbitals are given by

$$\psi_{2s}(\vec{r})=\frac{\exp^{-r/2}(2-r)}{\sqrt{32\pi}} \quad \psi_{2p_x}(\vec{r})=\frac{x\exp^{-r/2}}{\sqrt{32\pi}} \quad \psi_{2p_y}(\vec{r})=\frac{y\exp^{-r/2}}{\sqrt{32\pi}} \quad \psi_{2p_z}(\vec{r})=\frac{z\exp^{-r/2}}{\sqrt{32\pi}}$$

Let us then guess that the set of FODs, that minimize the energy are determined by a tetrahedron with vertices chosen such that $\psi_{2s}(\vec{a}\,) = \psi_{2p_x}(\vec{a}\,) = \psi_{2p_y}(\vec{a}\,) = \psi_{2p_z}(\vec{a}\,)$. The condition that allows for this equality is to choose FODS which satisfy

$$|a_x| = |a_y| = |a_z| = 2 - |a| \quad \text{with} \quad |a| = \sqrt{3}|a_x|$$

Under these conditions, it then follows that a choice for the FLOs is given by

$$\begin{aligned}
|F_1\rangle &= \frac{1}{2}\big(|\psi_{2s}\rangle + |\psi_{2p_x}\rangle + |\psi_{2p_y}\rangle + |\psi_{2p_z}\rangle\big) = \big|\varphi_1^{FLO}\big\rangle \quad ! \\
|F_2\rangle &= \frac{1}{2}\big(|\psi_{2s}\rangle - |\psi_{2p_x}\rangle - |\psi_{2p_y}\rangle + |\psi_{2p_z}\rangle\big) = \big|\varphi_2^{FLO}\big\rangle \quad ! \\
|F_3\rangle &= \frac{1}{2}\big(|\psi_{2s}\rangle - |\psi_{2p_x}\rangle + |\psi_{2p_y}\rangle - |\psi_{2p_z}\rangle\big) = \big|\varphi_3^{FLO}\big\rangle \quad ! \\
|F_4\rangle &= \frac{1}{2}\big(|\psi_{2s}\rangle + |\psi_{2p_x}\rangle - |\psi_{2p_y}\rangle - |\psi_{2p_z}\rangle\big) = \big|\varphi_4^{FLO}\big\rangle \quad !
\end{aligned}$$

In the above, the exclamation mark has been added because this choice of FODs leads to the rare, but sought-after, condition that the Fermi-orbital and Fermi-Löwdin orbital are in fact identical. A second rarity is that for this special case, the FLOs also satisfy the localization equations within their subspace. A third rarity, and curiosity, is that if the set of four FODs is broken up into two pairs of FODs, the Fermi-Löwdin orbitals are invariant as the vertices are pinched toward one another. As a first illustration, calculations on some closed shell atoms will be discussed. The appearance of hybridization is common within the FLO formalism and not limited to sp-hybridization. In Fig. 2, the sp^3d^5 and $sp^3d^5f^7$ hybrids that are found for systems like Kr and Rn are illustrated.

In columns 1–4 of Table 1, the total energies for rare-gas atoms and a few lighter atoms with closed spin shells are presented. For completeness we also include the Hartree-Fock value of the energy that is calculated with the self-consistent FLOSIC orbitals. In a later section, the possibility of complex FLOs is introduced and the fifth column of this table will be discussed in that section. In preparation for that discussion it is a useful exercise to consider the possibility of multiplying any of the $2s/2p$ orbitals by $\sqrt{-1} = i$. The reader can convince themselves that the resulting FLOs would still be orthonormal and therefore a viable local orbital set within the original formulation of the self-interaction correction.

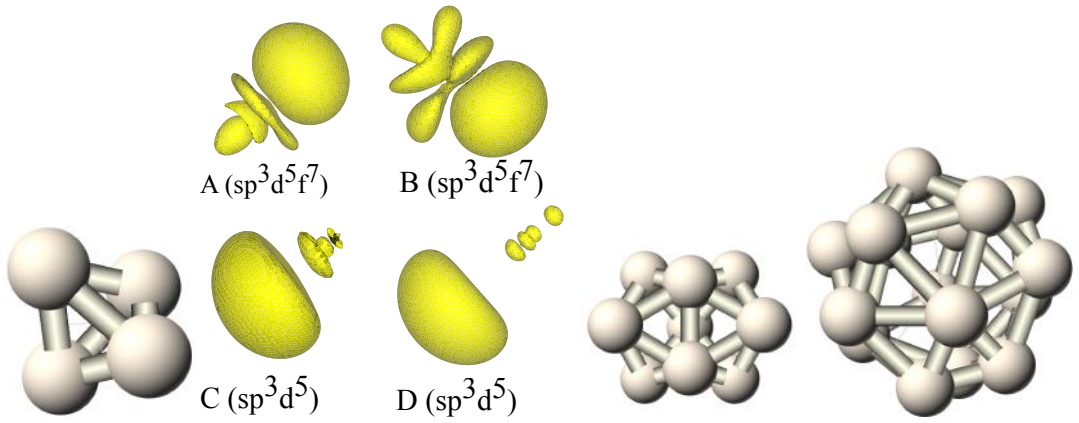

Fig. 2: *Relatively regularly polyhedra, referred to here as "flotonic solids", can be used for initializing FOD geometries that form a reciprocal lattice from closed shell atomic Kohn-Sham orbital sets. In this picture, isosurface plots of the orbital densities of inequivalent FLOs for the Radon $n = 4$ shells ($4s4p^3 4d^5 4f^7$, top) and $n = 3$ ($3s3p^3 3d^5$, bottom) shells. For the $n = 4$ shell, there are four FLOs that resemble FLO A and 12 FLOs that resemble FLO B. For the $n = 3$ shell, there are six FLOs that resemble FLO C and three FLOs that resemble FLO D. The flotonic solid for the $n = 2$ shell is a tetrahedron and it leads to standard sp^3 hybrids.*

Atom	HF (Ha)	Exp. (Ha)	LSDA (Ha)	rFLOSIC (Ha)	cFLOSIC (Ha)	ΔE (eV)
H	-0.5000	-0.500	-0.4786	-0.4999	-0.4999	0.00
He	-2.8615	-2.903	-2.8344	-2.9197	-2.9197	0.00
Li	-7.4320	-7.478	-7.3432	-7.5091	-7.5091	0.00
Be	-14.5715	-14.668	-14.4461	-14.7066	-14.7066	0.00
N	-54.3997	-54.612	-54.1342	-54.7407	-54.7578	-0.47
Ne	-128.5392	-129.053	-128.2297	-129.2805	-129.3339	-1.45
Ar	-526.7984	-528.223	-525.9395	-528.5365	-528.6767	-3.82
Kr	-2752.0206		-2750.1330	-2757.6071	-2758.0253	-11.39

Table 1: *Total energies (in Ha) of atoms from experiment, LSDA, rFLOSIC, cFLOSIC, and the total energy difference between the complex and real methods, ΔE = cFLOSICrFLOSIC (in eV). The cFLOSIC energies are evaluated using the self-consistent rFLOSIC electron density. Structures based upon the flotonic solids, described in the last section of this paper, appear to lead to the lowest energy solutions. It is only here that the Hartree-Fock energy has been systematically tracked as a function of the FLOSIC energy. So far it appears that the Hartree-Fock energy decreases as the FLOSIC energy decreases. (Calculations performed by Pederson and Withanage)*

2.2 The closed-shell N_2 molecule

The N_2 molecule, with a triple bond, is the second strongest diatomic molecule. Its isoelectronic cousin, carbon-monoxide, is slightly stronger due to similar covalent bonding and some degree of ionic enhancement. The molecule has cylindrical symmetry. Within the FLOSIC formulation, there are three inequivalent FODs given by $\vec{a}_{1s} = (0.628, 0.628, 0.628)$, $\vec{a}_{\textit{lone-pair}} = (1.311, 1.311, 1.311)$ and $\vec{a}_{\textit{banana}} = (0.702, -0.702, 0.000)$. To make contact with the discussion of sp^3 hybrids in the previous section, note that relative to the nitrogen atom, the lone-pair FOD

Mol.	LSD (PW92)	GGA (PBE)	FLOSIC-LSD (PW92)	Hartree-Fock	Expt
N_2	11.58	10.49	10.24	4.87	9.84

Table 2: *Atomization energies (eV) of N_2 as determined from LDA(PW92), GGA(PBE), FLOSIC-LSD(PW92), Hartree-Fock, and experiment. The same basis set is used for all calculations. For these calculations the nitrogen atoms were placed at the LDA equilibrium separation, at $R_\pm = \pm(0.598, 0.598, 0.598)$.*

and the three-equivalent banana-bond FODs form an almost perfect tetrahedron and thereby allow the nitrogen molecule to seamlessly dissociate into two atoms with anti-parallel spin polarization. The complete set of 14-FODs can be generated from the D_{3h} symmetry operations. Pictures of the resulting localized orbitals are shown in Fig. 3. The strongly covalent singlet N_2 molecule, $1\sigma_g^2 1\sigma_u^2 2\sigma_g^2 2\sigma_u^2 1\pi_u^4 3\sigma_g^2$, dissociates into an open-shell singlet with three unpaired $2p$ electrons per atom. For comparison, the LSD(PW92) energy functional gives an atomization energy of 11.54 eV at this bondlength and the GGA(PBE) energy functional gives an atomization energy of 10.54 eV. In Fig. 3, the valence FODs are shown pictorially. Complex FODs will be discussed in a later section. The real FODs $1s_{A\pm} = (1\sigma_g' \pm 1\sigma_u')/\sqrt{2}$, lone-pair states on the exterior of the molecule, $2sp_{A\pm} = (3\sigma_g' \pm 2\sigma_u')/\sqrt{2}$, and three bond-centered banana orbitals (e.g., $\varphi_n = \left(2\sigma_g' - \sqrt{2}[\cos(\frac{2n\pi}{3})\pi_{ux} + \sin(\frac{2n\pi}{3})\pi_{uy}]\right)/\sqrt{3}$, with $n = -1, 0, +1$). The primes indicate that KS molecular orbitals of the same symmetry are mixed together by a unitary transformation within each irreducible representation to minimize Eq. (1). For example the $\{2\sigma_g', 3\sigma_g'\}$ are not perfect eigenstates. Instead they are determined by a nearly diagonal unitary mixture of the $\{2\sigma_g, 3\sigma_g\}$ KS eigenstates.

In the earliest implementation of self-interaction corrections to molecules a similar construction of localized orbitals for the σ states was envisioned. However for the π-states, a symmetry argument was made that the energy density should have the same symmetry as the total density. This mandates using localized SIC orbitals for the π-states as $|\varphi_\pm\rangle = \left(|\psi_{\pi_{ux}}\rangle + i\,|\psi_{\pi_{uy}}\rangle\right)/\sqrt{2}$.

Comments on Symmetry Breaking: Beginning with the earliest origins of the use of SIC there have been assertions that the use of SIC breaks symmetry. Here we should mention that there is spin-symmetry breaking, often needed in ordinary density-functional approximations, for the description of bond breaking, which is needed for most approximations to the universal functional. It is further quite common to hear assertions that there is unphysical symmetry breaking within the FLOSIC method. The experience of this author is that, while the inclusion of self-interactions leads to slightly less numerical stability than is available in standard DFT calculations, it is generally possible to find a lower energy solution that exhibits higher symmetry. A caution to readers is that when minor symmetry breaking is observed, it will always be the case that a nearby symmetrical solution will be a critical point and the goal should be to determine whether such solutions are lower in energy. Further it should be noted that when broken symmetry solutions exist, especially for spin-ordered systems, the solutions generally contain information about low-lying excited states.

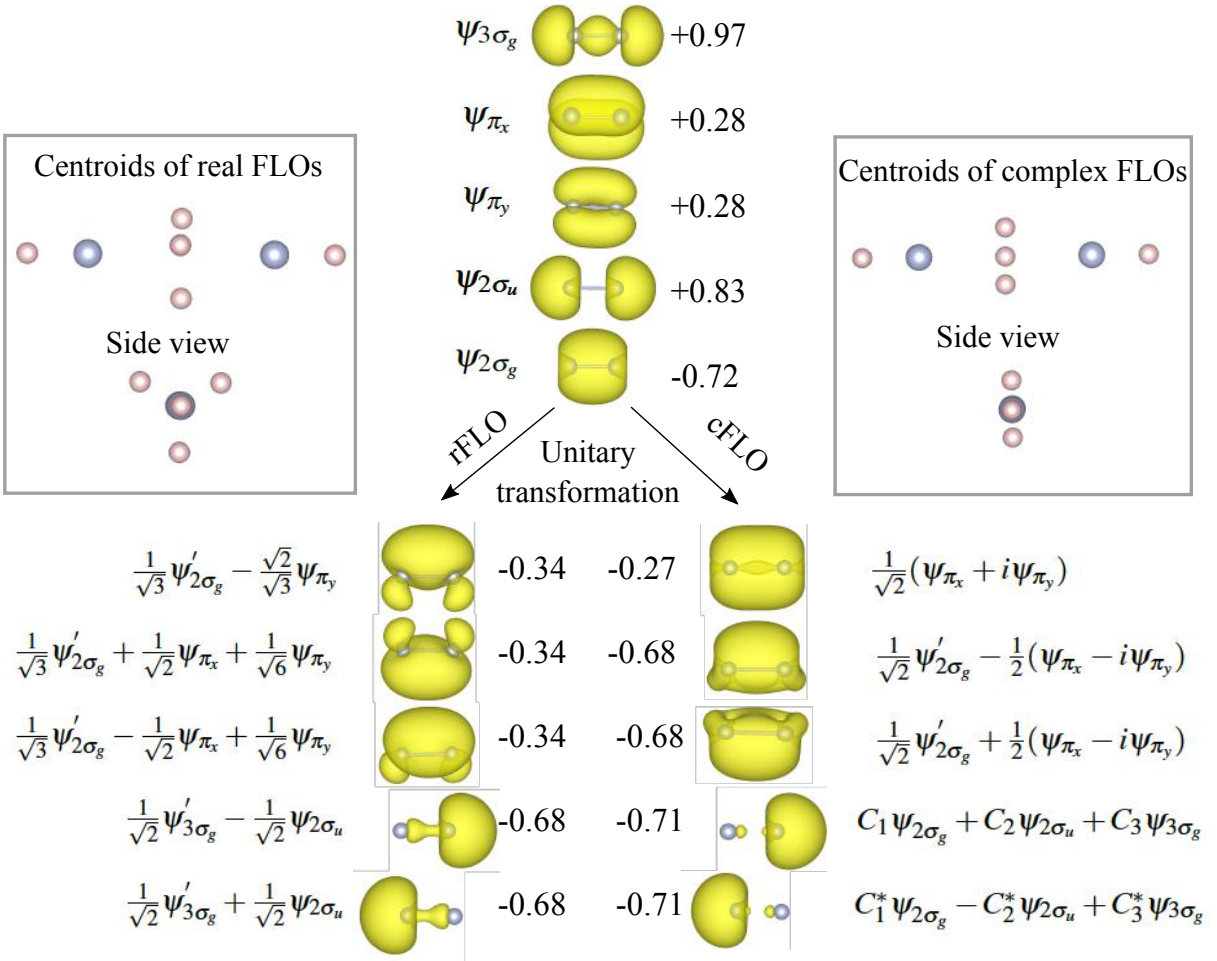

Fig. 3: *Valence orbital densities of N_2 for several different forms of density functional implementations. In the upper panel the standard canonical orbitals are shown. The shape of these orbitals have minimal variation regardless of functional choice (Exchange-Only, Perdew-Wang 92, PBE-GGA, Hartree-Fock, etc). When self-interaction corrections are included and orbitals are constrained to be real, the three bonding orbitals form banana bonds. These orbitals may be thought of as bonding combinations of sp^2 atomic orbitals) and this choice is, again, weakly dependent on the functional. However, if the constraint of reality is dropped and complex FODs are adopted, (cFLO) the orbitals soften their variability as shown on the far right. The SIC energy $E^{SIC}[n_{i\sigma}]$ (in eV) is indicated next to each orbital. The expansion of each rFLO and cFLO orbital in terms of the canonical orbitals is shown. The centroids of the rFLOs (left) and cFLOs (right) are indicated in the gray boxes. For the rFLOs, these correspond closely to the FOD positions. However, it is not generally true that the FOD position will correspond to the orbital centroid.*

2.3 A closed shell electron gas: Wannier functions, FLOs and FOs

Very early on, Wannier discovered a set of orthonormal functions, constructed from Bloch functions, that now bear his name. This work was accomplished prior to the computer age. Therefore, to make progress Wannier considered a uniform density gas. Rather that consider filling a Fermi-Sphere with plane waves, Wannier imagined approximating an insulating crystal by a cubic Brillouin zone. States on the inside of the "Wannier Cube" were occupied and states on

the outside were unoccupied. The title of his land-mark paper [3] is: *Structure of Electronic Excitation Levels in Insulating Crystals*. In it he wrote down Wannier functions of the form

$$\omega(r-R_\mu) = \frac{1}{\sqrt{\pi^3}} \prod_i \frac{\sin\left(q_F(x^i-X^i_\mu)\right)}{\sqrt{q_F}(x^i-X^i_\mu)}, \tag{4}$$

with $\boldsymbol{R}_\mu = (m_x, m_y, m_z)(\pi/q_F)$ and q_F is half the width of the cubic Brillouin zone. By inscribing the largest possible "Wannier cube" ($q_F = k_F/\sqrt{3}$) within the Fermi sphere, a specific set of Wannier functions may be derived. It has been shown early on by this author that this set of functions leads to a negative self-interaction correction for of the plane-wave states enclosed within the Wannier cube. So in the exchange-only limit, a limit that was perhaps the only tractable problem in 1937, it is highly probable that either exact exchange or the self-interaction correction would open up a HOMO-LUMO gap. By inspection, and related to the uncertainty principle, it is clear that the original Wannier functions get more localized as the magnitude of the q_F-vector gets larger. It is easy to verify that Wannier functions are a sub-class of the Fermi orbitals! The exclamation mark is included here because the original set of Wannier functions join the sp^3 hybrids as being an example where the Fermi orbitals are already orthogonal to one another. The possibility that, for any system, there is a set of FODs that leads to orthonormal FOs has been discussed and these orbitals were crowned "the most loved localized orbitals". To date there are very few exact cases, possibly only two, that satisfy this criterion. A few more comments illustrate their physical and chemical nature. At $\boldsymbol{r} = \vec{a}_{i\sigma}$, the value of the absolute square of the FO is identically equal to the total spin density at $\vec{r} = \vec{a}_{i\sigma}$. Further, the FO associated with any position, $\vec{a}_{i\sigma}$, in space is normalized to unity. Second, the absolute square of the FO is minus the exchange-hole density at $\boldsymbol{r}$ around an electron at $\vec{a}_{i\sigma}$. There have been several different attempts to find localized orbitals for the free-electron gas. Most of the work discussed in these references was in regard to the standard free-electron gas which leads to a set of occupied plane-wave states inside a Fermi sphere.

It is hypothesized that at low enough density, the limit of Wigner crystallization, despite the large increase in kinetic energy associated with the deformation of a spherical Fermi surface to a non-spherical Fermi surface, the derivative of the energy with respect to $n^{1/3}$ is more negative in the limit of $n \to 0$ (if the SIC-energy is indeed negative as is the case for the LSDA exchange-only functional). It was shown analytically that, in the low-uniform-density limit, a state that is based on a full band of plane waves/Wannier functions confined within a simple-cubic "Wannier cube" is lower in energy than the standard state composed of plane waves confined to the Fermi sphere. The author estimates that the crossover occurs at values of $\mathrm{r}_s > 35$ and that the uniform density "insulating state" (plane waves within a "Wannier cube") is lower than the metallic state. However with a new theorem that guarantees that one can find solutions of the $N-1$ electron problem when the N electron-problem is solved, it seems that some analytical progress toward defining FLOs for the metallic free-electron gas is now possible. Knowing this may very well determine if the sign of the SIC-energy of a localized orbital in the low-density limit must be negative.

3 Fermi-Löwdin orbitals: An existence proof and their construction

Given the infinite number of points, one expects that it would be rather easy to find a set of Fermi-orbital descriptors for construction of the Fermi-Löwdin orbitals. Further in the previous section, two simple examples requiring no computation have been shown to immediately provide FLOs – in fact the most loved ones.
In practice it is much more difficult to do than expected. Here we provide a proof that a solution always exists and that every time one initial solution is determined that an avalanche of solutions for smaller systems follows. To determine the Fermi-Löwdin orbitals one first constructs the overlap matrix

$$\underline{\mathrm{S}}_{ij} = \langle F_i | F_j \rangle = \frac{\sum_\alpha \psi_\alpha(\mathbf{a}_i)\psi_\alpha(\boldsymbol{a}_j)}{\sqrt{\rho(\boldsymbol{a}_i)\rho(\boldsymbol{a}_j)}} = \frac{\sum_\alpha W_{\alpha i} W_{\alpha j}}{\sqrt{\rho(\boldsymbol{a}_i)\rho(\boldsymbol{a}_j)}}\,. \tag{5}$$

Give the overlap matrix, an intermediate set of its eigenvectors is derived according to

$$\underline{\mathrm{S}}\,\vec{T}_\alpha = Q_\alpha \vec{T}_\alpha. \tag{6}$$

The eigenvectors Q_α must be greater than zero and $\sum_\alpha Q_\alpha = N$, the number of Kohn-Sham orbitals. The eigenvectors, $|T_\alpha\rangle$ are defined in terms of the Fermi orbitals according to $|T_\alpha\rangle = \sum_i |F_{\vec{a}}\rangle$, with $\sum_\alpha T_{\alpha i} T_{\alpha j} = \delta_{ij}$ and $\sum_i T_{\alpha i} T_{\beta_i} = \delta_{\alpha\beta}$. To obtain Fermi-Löwdin orbitals from these intermediate orbitals we first normalize them, $|T'_\alpha\rangle \rightarrow |T_\alpha\rangle/\sqrt{Q_\alpha}$, and then back-transform them according to

$$|\Phi_i^{FLO}\rangle = \sum_\alpha \frac{1}{\sqrt{Q_\alpha}}\, T_{\alpha i}\, |T_\alpha\rangle. \tag{7}$$

Because the T-matrix is unitary, it is clear that in the limit of small overlap the eigenvalues (Q_α) tend to unity and that $|\Phi_i^{FLO}\rangle \rightarrow |F_{\vec{a}_i}\rangle$. In the following section, several well-known cases in physics and chemistry are discussed. However, it is more common to find that some of the overlaps vanish and here the discussion focuses first on demonstrating that it is formally possible to find the Fermi-orbital overlaps. Subsequent to this discussion, ideas on how to find them for hard cases are included. To see that there is always a solution, let us start with Eq. (5) which relates the Fermi-orbital overlap matrix to the Kohn-Sham orbitals, and multiply both sides of the equation by $\sqrt{\rho(\vec{a_i})\rho(\vec{a_j})}$. We find

$$\sum_\alpha W_{\alpha i} W_{\alpha j} = \sqrt{\rho(\boldsymbol{a}_i)}\,\underline{\mathrm{S}}_{ij}\sqrt{\rho}(\boldsymbol{a}_j) = \sum_{pq} \sqrt{\rho(\boldsymbol{a}_p)}\;\delta_{ip}\;\underline{\mathrm{S}}_{pq}\;\delta_{qj}\;\sqrt{\rho(\boldsymbol{a}_j)}. \tag{8}$$

In the above equation $W_{\alpha i} = \psi_\alpha(\boldsymbol{a}_i)$, which reminds us that we can think of the left-hand side of the equation as a product of two matrices. The Kronecker delta function δ_{ip} is a convenient way to write the right-hand side as the product of three matrices. Since each element of the diagonal matrix, $\sqrt{\rho(\vec{a_p})}$ is now expressed as a manifestly positive definite matrix $P_{ip} \equiv \sqrt{\rho(\boldsymbol{a}_p)}\;\delta_{ip}$, Eq. (8) becomes, in matrix form,

$$\underline{\mathrm{W}} \times \underline{\mathrm{W}}^T = \underline{\mathrm{P}} \times \underline{\mathrm{S}} \times \underline{\mathrm{P}}^T, \tag{9}$$

and we can take the determinant of both sides which yields

$$\det(\underline{\mathrm{W}})^2 = \det(\underline{\mathrm{P}})^2 \det(\underline{\mathrm{S}}). \tag{10}$$

Inspection of the left-hand side of the equation shows that $\det(\underline{\mathrm{W}})$ is identically equal to the value of the many-electron Slater determinant, composed of the Kohn-Sham orbitals, evaluated at the geometry of the Fermi-orbital descriptors (multiplied by $\sqrt{N!}$). The $\det(\underline{\mathrm{P}})$ never vanishes except for the non-physical case that every Kohn-Sham orbital is zero at one or more FOD positions. Therefore the determinant of the FO-overlap matrix is not zero if $\det(W)$ is. Since the $\det(W)$ is the value of a Slater determinant constructed from the Kohn-Sham orbitals, a sufficient condition for obtaining a positive definite Fermi-orbital overlap matrix is that $\underline{\mathrm{W}}$ is invertible. Alternatively, a sufficient condition is that a many-electron wavefunction exists for the system. If a many-electron wavefunction exists, there must be at least one Slater determinant that is non-zero somewhere. Since the product of the eigenvalues of the FO-overlap matrix is identically equal to $\det(\underline{\mathrm{S}})$, it follows that a set of Fermi-Löwdin orbitals must exist if $\det(W)\neq 0$. Let us now rewrite the Slater-Determinant in terms of an alternative set of orbitals $\varphi_i = \sum U_{i\alpha}\psi_\alpha$. Since $\det(U\psi) = \det(U)\det(\psi)$, the many electron Slater determinant can, at most, change by a phase factor

$$\det \underline{\mathrm{W}} = \begin{vmatrix} \psi_1(\boldsymbol{a}_1) & \psi_2(\boldsymbol{a}_1) & \cdots & \psi_N(\boldsymbol{a}_1) \\ \psi_1(\boldsymbol{a}_2) & \psi_2(\boldsymbol{a}_2) & \cdots & \psi_N(\boldsymbol{a}_2) \\ \vdots & \vdots & \ddots & \vdots \\ \psi_1(\boldsymbol{a}_N) & \psi_2(\boldsymbol{a}_N) & \cdots & \psi_N(\boldsymbol{a}_N) \end{vmatrix} = e^{i\theta} \begin{vmatrix} \varphi_1(\boldsymbol{a}_1) & \varphi_2(\boldsymbol{a}_1) & \cdots & \varphi_N(\mathbf{a}_1) \\ \varphi_1(\boldsymbol{a}_2) & \varphi_2(\boldsymbol{a}_2) & \cdots & \varphi_N(\boldsymbol{a}_2) \\ \vdots & \vdots & \ddots & \vdots \\ \varphi_1(\boldsymbol{a}_N) & \varphi_2(\boldsymbol{a}_N) & \cdots & \varphi_N(\boldsymbol{a}_N) \end{vmatrix}. \tag{11}$$

The orbitals $(\varphi_1, \varphi_2, ...)$ can be any set of orbitals that are related to the Kohn-Sham orbitals (ψ_α) by a unitary transformation, including the FLOs, if the determinant of W is non-zero. In the above equation $e^{i\theta}$ would be the determinant of the unitary transformation. It follows that, if an N-electron wavefunction is not zero everywhere, there is at least one set of KS orbitals and one set of FODs for any non-zero N-electron wavefunction. Therefore it is guaranteed that it is always possible to find an initial set of KS orbitals and FODs. Once accomplished the gradient techniques discussed in Sec. 3.1 may be used reach a stationary point. It will be important for FLOSIC practitioners to learn when such stationary points are ground states and when they represent excitations.

An avalanche of solutions

Because it is in fact difficult to find a starting solution, it is then worthwhile to make the most out of every human-determined starting solution found. Here we consider the manifestations of finding one viable solution. Since an $N\times N$ determinant can be analytically represented in turns of a sum of N cofactors, it means that if an $N\times N$ determinant is non zero, that at least one of its co-factors ($N-1 \times N-1$ determinants) is non zero. This means that once *one* initial solution is found, a minimum of $N-1$ and a maximum of 2^N-2 new starting solutions are found for systems with fewer electrons. This provides a big advantage from the standpoint

of finding solutions. Further, once a non-positive-definite overlap matrix is found for a set of N-orthonormal orbitals, the resulting set of FLOs almost satisfy the following expression

$$\varphi_i^{FLO}(\boldsymbol{a}_j) \approx \sqrt{\rho(\boldsymbol{a}_i)}\,\delta_{ij}. \tag{12}$$

In terms of the ultimate goal of using quasi-classical electronic positions to better inform density-functional development, this proof suggests an alternative criterion for choosing FODs for defining the self-interaction correction (SIC). One could maximize the determinant of the FO-overlap matrix and then assert that the SIC energy is being defined by a region where the amplitude of the many-electron KS Slater determinant was large. However, for now, we stick to the necessity of subsequent optimization of the FODs based on energy minimization.

Existence proofs provide guarantees that solutions can be found but do not necessarily provide a set of directions on how to find them. We will return to strategies for finding initial starting points in a later section but first turn to the equations that are needed to find the optimal set of Fermi-orbital descriptors once an initial starting set has been found.

3.1 Optimizing Fermi orbital descriptors and Fermi-Löwdin orbitals using derivatives

Before embarking upon this section it is important to distinguish between Fermi-orbital descriptors (FODs) and Fermi-Löwdin-orbital centroids. FODs are the variational parameters. Fermi-Löwdin-orbital centroids correspond to the center of gravity $\langle\varphi_i^{FLO}|\vec{r}\,|\varphi_i^{FLO}\rangle$. The centroids are determined by the full set of descriptors. Sometimes, for example for sigma bonds, the FOD and FLOC are similar but generally this is not the case.

To efficiently use a Fermi-orbital based construction of localized orbitals in large systems it is necessary to have an analytic expression for the derivatives of the orbital-dependent energy terms with respect to these classical electronic positions. An additional goal for the next period of time should be to determine second derivatives of energy with respect to the Fermi-orbital descriptors (FODs). In the following the details that go into determining FOD gradients are discussed. The resulting equations depend on the evaluation of N sparse $N\times N$ matrices and one full $N\times N$ matrix. As such the evaluations of the FOD gradients and subsequent optimization of the SIC-DFT Hamiltonian is not necessarily more complicated than standard density-functional-based methods. For simplicity, spin indices on the orbitals and the spin-density matrices are suppressed. Since the goal of this section is to develop analytic expressions for transformations between various orbital sets, there are four different sets of orbitals that need to be considered. These four sets will were initially referred to as the Kohn-Sham orbitals (KS), the Fermi Orbitals (FO), the Intermediate Löwdin Orbitals (ILO), and the Localized Löwdin Orbitals (LLO), respectively [20, 21]. However, the nomenclature for the latter set is now Fermi-Löwdin Orbitals (FLOs). Also, in the original discussions of gradients [20, 21], the positions were imprecisely referred to as Fermi-orbital centroids rather than Fermi-orbital derivatives. The gradient of the FLO with respect to the FOD is needed to determine the optimal

Fermi-orbital descriptors for constructing the SIC energy. It is given by

$$\nabla_{\boldsymbol{a}_{i\sigma}} F_{i\sigma}(\boldsymbol{r}) = \frac{\sum_\alpha \psi^*_{\alpha\sigma}(\boldsymbol{r})\, \nabla_{\boldsymbol{a}_{i\sigma}} \psi_{\alpha\sigma}(\boldsymbol{a}_{i\sigma})}{\sqrt{\rho(\boldsymbol{a}_{i\sigma})}} - \frac{F_{i\sigma}(\boldsymbol{r}) \nabla_{\boldsymbol{a}_{i\sigma}} \rho(\boldsymbol{a}_{i\sigma})}{2\rho(\boldsymbol{a}_{i\sigma})} \tag{13}$$

$$= \sum_\alpha F^\alpha_{i\sigma} \left(\frac{\nabla_{\boldsymbol{a}_{i\sigma}} \psi_{\alpha\sigma}(\boldsymbol{a}_{i\sigma})}{\psi_{\alpha\sigma}(\boldsymbol{a}_{i\sigma})} - \frac{\nabla_{\boldsymbol{a}_{i\sigma}} \rho(\boldsymbol{a}_{i\sigma})}{2\rho(\boldsymbol{a}_{i\sigma})} \right) \quad \text{with} \quad F^\alpha_{i\sigma} \equiv \frac{\psi^*_{\alpha\sigma}(\boldsymbol{r}) \psi_{\alpha\sigma}(\boldsymbol{a}_{i\sigma})}{\sqrt{\rho(\boldsymbol{a}_{i\sigma})}}\,. \tag{14}$$

By construction, each of the FOs is normalized to unity and the set of Fermi orbitals spans the same space as the KS and FLO orbitals as long as the set of FODs, $a_{i\sigma}$, are far enough from one another. The ILO also span the space of the KS and FLO but they are neither orthogonal in orbital space nor normalized. The ILO are referred to as $|T_\alpha\rangle$ in the forthcoming equations. Their normalization, Q_α, is determined by the standard (i.e. non-general) diagonalization of the FO-overlap matrix according to

$$\sum_j S_{ij} T_{\alpha j} = Q_\alpha T_{\alpha i} \quad \text{where} \quad |T_\alpha\rangle = \sum_j T_{\alpha j} |F_j\rangle \quad \text{and} \quad S_{ij} = \langle F_i | F_j \rangle \tag{15}$$

The FLO, designated by φ_k, are then constructed from the ILO and their associated eigenvalues according to

$$|\varphi_k\rangle = \sum_{\alpha j} \frac{1}{\sqrt{Q_\alpha}} T_{\alpha k} T_{\alpha j} |F_j\rangle \equiv \sum_j \varphi^F_{kj} |F_j\rangle. \tag{16}$$

Because the FO overlap matrix is real and symmetric, the inverse transformation between Fermi orbitals and the FLO is also determined from

$$|F_l\rangle = \sum_{\beta n} T_{\beta l} \sqrt{Q_\beta} T_{\beta n} |\varphi_n\rangle. \tag{17}$$

Although no analytical use for the following equation has been identified, it is formally interesting and computationally useful to note that, since the FLO are unitarily equivalent to the KS orbitals, the Fermi orbitals may also be constructed from the FLO according to

$$F_{l\sigma}(\boldsymbol{r}) = \frac{\sum_n \varphi^*_{n\sigma}(\boldsymbol{r})\, \varphi_{n\sigma}(\boldsymbol{a}_{l\sigma})}{\sqrt{\sum_n |\varphi_{n\sigma}(\boldsymbol{a}_{l\sigma})|^2}} \equiv \sum_\alpha C^\sigma_{ln}\, \varphi_{n\sigma}(\boldsymbol{r}). \tag{18}$$

In other words, the inverse transformation coefficients determined by Eq. (17) are also determined by knowing the values of the FLO at the FODs. Possibly this equality could be used to derive something useful. Even if it is not found to be useful for analytic purposes, it is computationally useful since it shows that one can use a previous guess of FLOs to construct a new set of FO and that the resulting matrices will be sparse. Assuming an initial set of FODs, $\{\boldsymbol{a}_m\}$, have been determined the derivative of the total SIC energy with respect to a specific FOD is

given by

$$\frac{dE^{SIC}}{da_m} = \sum_k \Big(\langle \frac{d\varphi_k}{da_m} | V^k_{SIC} | \varphi_k \rangle + \langle \varphi_k | V^k_{SIC} | \frac{d\varphi_k}{da_m} \rangle \Big) \tag{19}$$

$$= \sum_{kl} \Big(\langle \frac{d\varphi_k}{da_m} | \varphi_l \rangle \langle \varphi_l | V^k_{SIC} | \varphi_k \rangle + \langle \varphi_k | V^k_{SIC} | \varphi_l \rangle \langle \varphi_l | \frac{d\varphi_k}{da_m} \rangle \Big) \tag{20}$$

$$= \sum_{kl} \lambda^k_{kl} \Big(\langle \frac{d\varphi_k}{da_m} | \varphi_l \rangle + \underbrace{\langle \varphi_l | \frac{d\varphi_k}{da_m} \rangle + \langle \frac{d\varphi_l}{da_m} | \varphi_k \rangle}_{= d\langle \varphi_l | \varphi_k \rangle / da_m} - \langle \frac{d\varphi_l}{da_m} | \varphi_k \rangle \Big) \tag{21}$$

$$= \sum_{kl} \lambda^k_{kl} \Big(\langle \frac{d\varphi_k}{da_m} | \varphi_l \rangle - \langle \frac{d\varphi_l}{da_m} | \varphi_k \rangle \Big) \equiv \sum_{kl}{}' \, \lambda^k_{kl} \, \Delta_{lk,m}, \tag{22}$$

with $\lambda^k_{kl} \equiv \langle \varphi_l | H_o + V^{SIC}_k | \varphi_k \rangle$. This is a general formula that does not depend on the Kohn-Sham orbitals being eigenstates of any Hamiltonian. Eq. (22) follows from Eq. (19) because the FO construction does not allow a FO to escape the space of the KS or FLO. In cases where one is determining analytic derivatives (such as Hellmann-Feynman forces), the orthonormality of the KS orbitals and the symmetry of the Lagrange-multiplier matrix leads to a simplification of the derivatives. In this more complicated case, the derivative of a FLO with respect to a FOD is determined by differentiating Eq. (16) and remembering that Q_α and $T_{\alpha k}$ depend on the entire set of FODs, $\{\vec{a}_m\}$, for any value of k but that the FO is only dependent on its own FOD. Since $|\varphi_k\rangle = \Sigma_{\alpha j} \frac{1}{\sqrt{Q_\alpha}} T_{\alpha k} T_{\alpha j} |F_j\rangle$ and remembering that only F_m depends on a_m, it follows that

$$\Big| \frac{d\varphi_k}{da_m} \Big\rangle = |D_{1,km}\rangle + |D_{2,km}\rangle + |D_{3,km}\rangle \equiv \sum_l \Delta^m_{kl} \, |\varphi_l\rangle \tag{23}$$

$$|D_{1,km}\rangle = \sum_{\alpha j} \frac{1}{\sqrt{Q_\alpha}} T_{\alpha k} T_{\alpha j} \Big| \frac{dF_j}{da_m} \Big\rangle = \sum_\alpha \frac{1}{\sqrt{Q_\alpha}} T_{\alpha k} T_{\alpha m} \Big| \frac{dF_m}{da_m} \Big\rangle \tag{24}$$

$$|D_{2,km}\rangle = -\frac{1}{2} \sum_{\alpha j} \frac{1}{Q^{3/2}_\alpha} \frac{dQ_\alpha}{da_m} T_{\alpha k} T_{\alpha j} |F_j\rangle \tag{25}$$

$$|D_{3,km}\rangle = \sum_{\alpha j} \frac{1}{\sqrt{Q_\alpha}} \Big(\frac{dT_{\alpha k}}{da_m} T_{\alpha j} + T_{\alpha k} \frac{dT_{\alpha j}}{da_m} \Big) |F_j\rangle \tag{26}$$

Each term $|D_{n,km}\rangle$ for $n = 1, 2, 3$ in the above equation is discussed separately:

Term 1

To determine the direct part of the FOD derivative, according to Eq. (22), the interest is in determining the difference of the matrix elements $\langle \varphi_l | D_{1,km} \rangle - \langle \varphi_k | D_{1,lm} \rangle$ which, using the expansion for the FLO in terms of the FO, Eq. (16), ($|\varphi_l\rangle = \sum_{\beta n} \frac{1}{\sqrt{Q_\beta}} T_{\beta l} T_{\beta n} |F_n\rangle$), can be rewritten as

$$\langle \varphi_l | D_{1,km} \rangle = \sum_\alpha \frac{T_{\alpha k} T_{\alpha m}}{\sqrt{Q_\alpha}} \langle \varphi_l | \frac{dF_m}{da_m} \rangle = \sum_{\alpha \beta n} \frac{T_{\alpha k} T_{\alpha m}}{\sqrt{Q_\alpha}} \frac{T_{\beta l} T_{\beta n}}{\sqrt{Q_\beta}} \langle F_n | \frac{dF_m}{da_m} \rangle \tag{27}$$

The difference of these two terms is then given by

$$\Delta^1_{lk,m} \equiv \langle\varphi_l|D_{1,km}\rangle - \langle\varphi_k|D_{1,lm}\rangle = \sum_{\alpha\beta n} \frac{T_{\alpha k}T_{\alpha m}T_{\beta l}T_{\beta n} - T_{\alpha l}T_{\alpha m}T_{\beta k}T_{\beta n}}{\sqrt{Q_\alpha Q_\beta}} \big\langle F_n\big|\frac{dF_m}{da_m}\big\rangle \tag{28}$$

$$= \sum_{\alpha\beta n} \frac{\big(T_{\alpha k}T_{\beta l} - T_{\alpha_l}T_{\beta k}\big)T_{\alpha m}T_{\beta n}}{\sqrt{Q_\alpha Q_\beta}} \big\langle F_n\big|\frac{dF_m}{da_m}\big\rangle. \tag{29}$$

Using $\varphi^F_{kj} = T_{\alpha k}T_{\alpha j}/\sqrt{Q_\alpha}$ defined in Eq. (16), it can be rewritten in the manifestly sparse form

$$\Delta^1_{lk,m} = \sum_n \big(\varphi^F_{km}\varphi^F_{ln} - \varphi^F_{lm}\varphi^F_{kn}\big)\big\langle F_n\big|\frac{dF_m}{da_m}\big\rangle = \varphi^F_{km}\big\langle\varphi_l\big|\frac{dF_m}{da_m}\big\rangle - \varphi^F_{lm}\big\langle\varphi_k\big|\frac{dF_m}{da_m}\big\rangle. \tag{30}$$

Term 2

Term 2 always vanishes: The term that is due to the gradient of the ILO eigenvalue with respect to a Fermi-orbital position becomes, inserting the expression for $|F_j\rangle$ given in Eq. (17)

$$|D_{2,km}\rangle = -\frac{1}{2}\sum_{\alpha j}\frac{1}{Q_\alpha^{3/2}}\frac{dQ_\alpha}{da_m}T_{\alpha k}T_{\alpha j}|F_j\rangle = -\frac{1}{2}\sum_{\alpha j\beta n}\frac{1}{Q_\alpha^{3/2}}\frac{dQ_\alpha}{da_m}T_{\alpha k}T_{\alpha j}\ T_{\beta j}\sqrt{Q_\beta}T_{\beta n}|\varphi_n\rangle. \tag{31}$$

It may be further simplified using the orthonormality of the ILOs, $\sum_j T_{\beta j}T_{\alpha j} = \delta_{\alpha\beta}$,

$$|D_{2,km}\rangle = -\frac{1}{2}\sum_{\alpha n}\frac{1}{Q_\alpha^{3/2}}\frac{dQ_\alpha}{da_m}T_{\alpha k}\sqrt{Q_\alpha}T_{\alpha n}|\varphi_n\rangle = -\frac{1}{2}\sum_{\alpha n}\frac{1}{Q_\alpha}\frac{dQ_\alpha}{da_m}T_{\alpha k}T_{\alpha n}|\varphi_n\rangle \tag{32}$$

so that, from the orthonormality, $\langle\varphi_l|\varphi_n\rangle = \delta_{ln}$, it follows that

$$\langle\varphi_l|D_{2,km}\rangle - \langle\varphi_k|D_{2,lm}\rangle - \frac{1}{2}\sum_\alpha\frac{1}{Q_\alpha}\frac{dQ_\alpha}{da_m}\big(T_{\alpha k}T_{\alpha l} - T_{\alpha l}T_{\alpha k}\big) = 0. \tag{33}$$

Term 3

In Ref. [20, 21] it was demonstrated that the analytical expression for the vector $\Delta_{kl,m}$ can be determined from sparse matrix manipulations and that the memory requirements scale better than N^2. In the above equations, the contributions from the direct $|D_{1,km}\rangle$ are analogous to the standard Hellmann-Feynman derivative since it arises from the explicit dependence of the FLO on the FOD. The terms involving $|D_{3,km}\rangle$ are more complicated. Qualitatively, these terms would be zero if there was a Hellmann-Feynman theorem or alternatively if the FLO actually satisfied the localization equations. However, because the FO-based formulation of the PZ-SIC already leads to unitary invariance there is neither required nor correct to force the localization equations [9, 11] need to be satisfied. The sum of the eigenvalues Q_α is always equal to the dimension of the KS space. The eigenvalues are bounded from below by zero and above by the dimension of the KS space. For reasonable guesses of the FODs, the eigenvalues are close to unity. For now, to make analytical progress, it is a assumed that FODs have been chosen that break all degeneracies of the FO-overlap derivatives, or that a small perturbation that breaks all

degeneracies has been added to Eq. (15). Then, a first-order perturbation analysis of Eq. (15) can be used

$$\frac{dT_{\alpha k}}{da_m} = \sum_{\beta\neq\alpha} T_{\beta k}\frac{\langle T_\beta|\frac{dS}{da_m}|T_\alpha\rangle}{Q_\alpha - Q_\beta} \tag{34}$$

to determine that

$$|D_{3,km}\rangle = \sum_j |F_j\rangle \sum_{\alpha,\beta\neq\alpha} \frac{\langle T_\beta|\frac{dS}{da_m}|T_\alpha\rangle}{Q_\alpha^{1/2}(Q_\alpha - Q_\beta)}\big(T_{\beta k}T_{\alpha j} + T_{\alpha k}T_{\beta j}\big) \tag{35}$$

$$= \sum_j |F_j\rangle \sum_{\alpha,\beta>\alpha} \frac{\langle T_\beta|\frac{dS}{da_m}|T_\alpha\rangle}{(Q_\alpha - Q_\beta)}\big(T_{\beta k}T_{\alpha j} + T_{\alpha k}T_{\beta j}\big)\left(\frac{1}{Q_\alpha^{1/2}} - \frac{1}{Q_\beta^{1/2}}\right) \tag{36}$$

$$= \sum_j |F_j\rangle \sum_{\alpha,\beta>\alpha} \frac{\langle T_\beta|\frac{dS}{da_m}|T_\alpha\rangle\big(T_{\beta k}T_{\alpha j}+T_{\alpha k}T_{\beta j}\big)(Q_\beta^{1/2}-Q_\alpha^{1/2})}{(Q_\alpha - Q_\beta)(Q_\alpha Q_\beta)^{1/2}} \tag{37}$$

$$= -\sum_j |F_j\rangle \sum_{\alpha,\beta>\alpha} \frac{\langle T_\beta|\frac{dS}{da_m}|T_\alpha\rangle\big(T_{\beta k}T_{\alpha j}+T_{\alpha k}T_{\beta j}\big)}{(Q_\alpha^{1/2}+Q_\beta^{1/2})(Q_\alpha Q_\beta)^{1/2}} \tag{38}$$

$$= -\sum_n |\varphi_n\rangle \sum_{\alpha,\beta>\alpha} \frac{\langle T_\beta|\frac{dS}{da_m}|T_\alpha\rangle\big(T_{\beta k}T_{\alpha n}Q_\alpha^{1/2}+T_{\alpha k}T_{\beta n}Q_\beta^{1/2}\big)}{(Q_\alpha^{1/2}+Q_\beta^{1/2})(Q_\alpha Q_\beta)^{1/2}} \tag{39}$$

where in the last step we have used Eq. (17) and the orthonormality $\sum_j T_{\beta j}T_{\alpha j} = \delta_{\alpha\beta}$

$$\sum_j \big(T_{\beta k}T_{\alpha j}+T_{\alpha k}T_{\beta j}\big)|F_j\rangle = \sum_{\gamma n j} \big(T_{\beta k}T_{\alpha j}+T_{\alpha k}T_{\beta j}\big)T_{\gamma j}Q_\gamma^{1/2}T_{\gamma n}|\varphi_n\rangle \tag{40}$$

$$= \sum_n \big(T_{\beta k}T_{\alpha n}Q_\alpha^{1/2}+T_{\alpha k}T_{\beta n}Q_\beta^{1/2}\big)|\varphi_n\rangle. \tag{41}$$

It is noted that at the end of the analysis there is no division by zero in the first-order perturbative expressions even when the energy denominator vanishes! Now, to circle back to Eq. (22), it is possible to evaluate the difference

$$\Delta^3_{lk,m} \equiv \langle\varphi_l|D_{3,lm}\rangle - \langle\varphi_k|D_{3,lm}\rangle \tag{42}$$

$$= -\frac{1}{2}{\sum_{\alpha\beta}}' \frac{\langle T_\beta|\frac{dS}{da_m}|T_\alpha\rangle\Big(\big(T_{\beta k}T_{\alpha n}Q_\alpha^{1/2}+T_{\alpha k}T_{\beta n}Q_\beta^{1/2}\big)-\big(T_{\beta k}T_{\alpha n}Q_\alpha^{1/2}+T_{\alpha k}T_{\beta n}Q_\beta^{1/2}\big)\Big)}{(Q_\alpha^{1/2}+Q_\beta^{1/2})(Q_\alpha Q_\beta)^{1/2}}$$

$$= -\frac{1}{2}{\sum_{\alpha\beta}}' \frac{\langle T_\beta|\frac{dS}{da_m}|T_\alpha\rangle}{(Q_\alpha^{1/2}+Q_\beta^{1/2})(Q_\alpha Q_\beta)^{1/2}}\big(T_{\alpha k}T_{\beta l} - T_{\alpha l}T_{\beta k}\big)\big(Q_\beta^{1/2}-Q_\alpha^{1/2}\big). \tag{43}$$

Expanding

$$\big\langle T_\beta\big|\frac{dS}{da_m}\big|T_\alpha\big\rangle = \sum_i \Big(T_{\beta i}\frac{dS_{im}}{da_m}T_{\alpha m} + T_{\beta m}\frac{dS_{mi}}{da_m}T_{\alpha i}\Big) = \sum_i \frac{dS_{im}}{da_m}\big(T_{\beta i}T_{\alpha m} + T_{\beta m}T_{\alpha i}\big) \tag{44}$$

and combining the above two equations together a computationally useful expression is found:

$$\Delta^3_{lk,m} = \frac{1}{2}\sum_{\alpha\beta i}\frac{dS_{im}}{da_m}\big(T_{\beta i}T_{\alpha m}+T_{\beta m}T_{\alpha i}\big)\big(T_{\alpha k}T_{\beta l}-T_{\alpha l}T_{\beta k}\big)\frac{Q_\alpha^{1/2}-Q_\beta^{1/2}}{(Q_\alpha^{1/2}+Q_\beta^{1/2})(Q_\alpha Q_\beta)^{1/2}}\,. \tag{45}$$

The above forms reduce the expression to the calculation of quantities that are symmetric under interchange of α and β and in terms of quantities that exhibit the sparsity. It shows that, if the calculation is performed in terms of Kohn-Sham eigenstates, the calculation of the derivatives may scale as poorly as N^4 in the small N limit. However, if one constructs the FOs in terms of the FLOs, the T matrix then becomes sparse and each bracketed quantity scales as N^2. The sparsity of the FLO SIC matrix elements ($\langle\varphi_k|H_o+V_k^{SIC}|\varphi_l\rangle$ already shows that one never needs to calculate all possible products of $T_{\alpha k}T_{\beta l}$. It is also noted that one does not need to calculate the contributions due to H_o since that contribution to the λ_{ij}^i matrices is always symmetric. To determine the final derivatives one simply evalutates $\Delta_{lk,m}$ in Eq. (22) according to

$$\Delta_{lk,m} = \Delta_{lk,m}^1 + \Delta_{lk,m}^3. \tag{46}$$

Once the gradients are calculated, the great expectation was that it would be as easy to step to the local minimum as it is for gradient-based optimizations of molecular, cluster, and solid-state geometries. While it is probably the case that the best possible optimization method has not been found, some lessons from optimization of molecular geometries still hold. First, as is the case for molecular geometries, the LBFGS method (implemented in FLOSIC by Jackson and Withanage) is generally more efficient than conjugate-gradient when one is reasonably close to a solution. Second, the use of approximations of second derivatives, determined by atomic calculations but then used for all systems, also provides for more efficient stepping to the minimum. Finally, the use of conjugate-gradient methods is more stable when one is far from solution as is the case for the optimization of molecular geometries. Additional efforts are being made to more efficiently use force information. A final comment is that since $\frac{d^m\langle\varphi_k|\varphi_l\rangle}{da_p^m} = 0$ for any values of m, k, l, and p, it is possible that higher order analytic derivatives can be determined in the frozen density regime.

3.2 Complex Fermi-orbital descriptors and complex Fermi-Löwdin orbitals

In one of the earliest applications of SIC to molecules, Pederson [9] suggested that the bonding π_u states should be complex to ensure that the symmetry was not broken. Early consideration of complex orbitals by Klüpfel *et al.* [18] were based on an energy minimization. The Fermi orbital is explicitly real if it is possible to represent the Kohn-Sham orbitals as real orbitals and if the FODs are constrained to be real. So in this sense the 2014 version of FLOSIC represented a self-consistent real theory. This section introduces the use of complex Fermi-orbital descriptors (FODs) in the Fermi-Löwdin self-interaction-corrected density functional theory (FLOSIC). With complex FODs, the Fermi-Löwdin orbitals (FLOs) used to evaluate the SIC correction to the total energy become complex. Complex FLO-SIC (cFLOSIC) calculations based on the local spin density approximation generally produce lower total energies than those found with FLOSIC restricted to real orbitals (rFLOSIC). The cFLOSIC results are qualitatively similar to earlier energy-localized Perdew-Zunger SIC (PZ-SIC) calculations using complex orbitals [18]. The energy lowering stems from the exchange-correlation part of the self-interaction correction.

The Hartree part of the correction is more negative in rFLOSIC. The energy difference between real and complex solutions is greater for more strongly hybridized FLOs in atoms and for FLOs corresponding to double- and triple-bonds in molecules. The case of N_2 is examined in detail to show the differences between the real and complex FLOs. We show that the complex triple-bond orbitals are simple and physically appealing combinations of π and σ_g orbitals that have been discussed only recently [25]. Consideration of complex FODs, and resulting unitary transformations, underscores the fact that FLO centroids are not necessarily good guesses for FOD positions in a FLOSIC calculation (It is for this reason that we pointed out earlier that the use of the term Fermi-orbital centroids was imprecise). Another reason to introduce complex FODs into FLOSIC is more practical. Gradient searches for optimal FOD positions fail when the FODs obtained at a given step in the search produce Fermi orbitals that are not linearly independent. Transition metal systems are particularly prone to this problem because the $n = 3$ orbitals have considerable spatial overlap. Complex FODs provide a larger parameter space and lead to smoother, numerically more tractable, orbitals. Using complex FODs as starting points helps avoid non-positive-definite FO-overlap matrices and makes the search process more efficient. The complex Fermi orbitals are defined by

$$F_i(\boldsymbol{r}) = \frac{\sum_\alpha \psi^*_\alpha(\boldsymbol{a}_i+\mathrm{i}\boldsymbol{b}_i)\psi_\alpha(\boldsymbol{r})}{\sqrt{\sum_\alpha \psi^*_\alpha(\boldsymbol{a}_i+\mathrm{i}\mathbf{b}_i)\psi_\alpha(\boldsymbol{a}_i+\mathrm{i}\boldsymbol{b}_i)}}\,. \tag{47}$$

In the above, the FODs are allowed to be complex, $\boldsymbol{a}_i+\mathrm{i}\boldsymbol{b}_i$. Evaluating the ψ_α at complex positions leads to complex Fermi orbitals, F_i. The complex FOs have the same, and orthonormal complex FLOs (cFLOs) have similar characteristics. In calculations using Gaussian-type basis functions, evaluating $\psi_\alpha(\boldsymbol{a}_i+\mathrm{i}\boldsymbol{b}_i)$ gives rise to positive exponential terms that can cause numerical difficulties. Because the terms appear in the numerator and denominator, they can be managed if handled carefully. Within a Gaussian-orbital construction, the wave function is ultimately decomposed in terms of polynomials (which become complex in cFLOSIC) and Gaussian envelope functions of the form $\exp(-\beta(\boldsymbol{a}_i+\mathrm{i}\boldsymbol{b}_i-\boldsymbol{A})^2)$, where $\boldsymbol{A}$ usually coincides with the position of an atom. The real part of the exponent becomes $-\beta(|\boldsymbol{a}_i-\boldsymbol{A}|^2-|\boldsymbol{b}_i|^2)$. In general, the values of β span many orders of magnitude ranging from 0.02 to approximately $50\,Z^{10/3}$ for atomic number Z. There is a combination of the quantities $\{\beta, \mathbf{A}, \boldsymbol{a}_i+\mathrm{i}\boldsymbol{b}_i\}$ that leads to the most positive exponent Γ_{max} that can be determined by sweeping through all combinations of Gaussian decay parameters, atomic positions, and FOD parameters. Γ_{max} can then be subtracted from all the exponents in the Gaussians prior to evaluating the exponential. This effectively multiplies the numerator and denominator of Eq. (47) by the same number and ensures that none of the terms diverge prior to division. This has no effect on the computer time. A similar approach will be needed for plane-wave basis functions (which as noted elsewhere will be interesting for finding FLOs for metallic model systems). In such cases, the envelope functions would have the form $\exp(\boldsymbol{k}\boldsymbol{b}_i)$. Again, multiplying and dividing each plane wave by the appropriate largest exponential will ensure that there are no numerical problems associated with exponentiation. For starting guesses, it is possible to choose the imaginary part of the FOD such that:$|\mathbf{b_i}| < |\mathbf{a_i}-\mathbf{A}|$, where $\mathbf{A}$ is the nuclear position closest to $\mathbf{a_i}$, to ensure decaying functions. One way to do this

is to choose $\boldsymbol{b}_i = \cos(\alpha)|\boldsymbol{A}-\boldsymbol{a}_i|\boldsymbol{u}$ with $\boldsymbol{u} = \big(\sin(\theta)\cos(\phi), \sin(\theta)\sin(\phi), \cos(\theta)\big)$. For the cFLOSIC results shown below, the FOD positions, $\boldsymbol{a}_i+\boldsymbol{b}_i$, are updated using a gradient optimization scheme. To optimize the complex FOD positions, we began by adding small random imaginary parts to the optimized (real) FODs from the corresponding rFLOSIC calculation. For each atom or molecule studied, 100 random complex FOD sets were generated. For each, the cFLOs were created and the corresponding SIC energies were calculated. The set with the lowest SIC energy was chosen as the starting point for a gradient optimization using energy gradients corresponding to both the real and imaginary parts of the FODs. The gradients corresponding to the imaginary parts required computing a numerical derivative of the orbital with respect to the component. The basis sets and integration grids used in the rFLOSIC and cFLOSIC calculations reported here were identical.

3.3 Atoms

Table 1 presents the total energies of atoms from Hartree-Fock LSDA, rFLOSIC and cFLOSIC calculations in Hartree (Ha) units. The energy difference cFLOSIC – rFLOSIC is also shown in electron volts (eV) for each atom. For most of the atoms in Table 1 the LSDA total energy is higher than the experimental reference energy, while the rFLOSIC and cFLOSIC total energies are lower. Thus both rFLOSIC and cFLOSIC correct the atomic total energies in the right direction, but often over-correct. The rFLOSIC and cFLOSIC total energies are identical up to Be. After that, the cFLOSIC energies are always lower. For Ne, Ar, and Kr, for example, the cFLOSIC energy is lower by -1.45, -3.82, and -11.39 eV, respectively. The Jackson-Withanage analysis can be used to identify how close the FLOSIC energies are to the SIC calculations with full variational freedom. They previously compared the FLOSIC method against the traditional implementation of PZ-SIC with full variational freedom (where a localization condition is invoked, known as the SIC-LE method) and have shown that rFLOSIC orbitals satisfy the LEs (symmetric Lagrange multiplier matrix) up to carbon. In real FLOSIC, the number of constraints is $3N$ where N is the number of occupied orbitals while the number of constraints in real orbital SIC-LE is $N(N-1)/2$. We find that orbitals from cFLOSIC (where the number of constraints is $6N$) satisfy the LEs (Hermitian Lagrange multiplier matrix) for complex orbital SIC up to Ne with or without freezing the $1s$ FOD. We understand that this is due to the added variational freedom due to the complex FODs.

Since the rFLOSIC and cFLOSIC total energies in Table 1 are evaluated based on the same total electron density, the DFT parts of the energies are the same and any differences are entirely due to the SIC corrections. In Ref. [25] the values of the corrections for the valence electron local orbitals of selected first row atoms are shown. Values for $n = 3$ and $4s$ local orbitals for Zn are also shown. The corrections are shown for both the majority and minority spin channels (for the spin-polarized cases). For the first-row atoms, the local orbitals are hybrids of $2s$ and $2p$ canonical orbitals. The Zn $n = 3$ local orbitals are hybrids of $3s$, $3p$, and $3d$ canonical orbitals. The canonical orbitals contributing most to each FLO are listed in the table. The magnitude of the orbital corrections increases across the first row atoms as the orbitals become more compact

	$-\sum_i U_C[n_i]$		$-\sum_i U_{xc}[n_i]$	
Atom	rFLOSIC (eV)	cFLOSIC (eV)	rFLOSIC (eV)	cFLOSIC (eV)
Ne	-296.03	-288.49	267.44	258.44
Ar	-704.76	-683.55	634.10	609.07
Kr	-2046.10	-1962.77	1842.74	1748.02

Table 3: *The total self-Hartree and self-exchange-correlation contributions to the total SIC energy (in eV) for the closed-shell atoms Ne, Ar, and Kr. The cFLOSIC energies were obtained from calculations using the self-consistent rFLOSIC electron densities.*

with increasing atomic number. For example, for the Be $2s$ orbital, the correction is -0.17 eV in both theories. For the N $2s2p^3$ FLO, the correction is -0.60 and -0.71 eV for rFLOSIC and cFLOSIC, respectively. For the Ne $2s2p^3$ FLO the corrections are -1.02 and -1.20 eV. For the $n = 3$ Zn FLOs the corresponding corrections are -1.35 and -1.58 eV and for the $n = 4$ FLO, -0.10 and -0.11 eV. The difference between the cFLOSIC and rFLOSIC corrections depends on the nature of the FLO. For s-type FLOs, the corrections are equal in the two approaches. The difference increases with increasing p-character in the FLO. For example, for the $2s$ and $2sp$ FLOs of Be and B, the corrections are essentially equal for the cFLO and rFLO. For the C $2sp^2$ FLOs, the cFLO correction is -0.02 eV lower than for the rFLO. For the N $2s2p^3$ FLO, the cFLO correction is -0.11 eV lower than for the rFLO. Similarly, for the minority spin FLOs of F the $2sp^2$ cFLO correction is -0.04 eV lower than for the rFLO, while for the Ne $2s2p^3$, the cFLO is -0.18 eV lower than the rFLO. Finally, for the Zn $3s3p^33d^5$ FLOs, the cFLO corrections are -0.23 eV lower than the rFLO. Figure 2 shows iso-surface plots of the rFLO orbital densities, $n = \varphi^2$. (Only the density for first FLO listed for each atom is shown.) For the cFLOs, iso-surface plots of $\varphi_R^2 - \varphi_I^2$ may be found in Ref. [25]. These plots highlight an effective smoothing of the FLOs, referred to as lobedness by Perdew, that may be an important issue for higher-level functionals. The SIC corrections include self-Hartree and self-exchange-correlation components. The former are negative, while the latter are positive. Table 3 shows the total self-Hartree and self-exchange-correlation parts of the SIC corrections separately for the representative atoms Ne, Ar, and Kr. The self-Hartree contributions are more negative in rFLOSIC in every case. This implies that the rFLOs are more localized than the cFLOs. On the other hand, the self-exchange-correlation energies are less positive for cFLOSIC. The combined corrections are more negative in cFLOSIC than rFLOSIC, as seen in Table 1. This implies that the cFLOSIC – rFLOSIC difference between the self-exchange-correlation components must be more negative that the self-Hartree difference is positive. For Ne, for example, the rFLOSIC self-Hartree component is 7.54 eV more negative, while the cFLOSIC overall correction is 1.45 eV more negative (cf. Table 1). Thus, the magnitude of the self-exchange energy for Ne is 8.99 eV smaller in cFLOSIC than rFLOSIC. Allowing complex degrees of freedom does not result in more localized atomic orbitals, but instead decreases the magnitude of the self-exchange-correlation energy of the orbitals.

Molecule	HF	LSDA	rFLOSIC(g)	rFLOSIC	cFLOSIC	Δ E (eV)
Li_2	-14.8693	-14.7237	-15.0561	-15.0561	-15.0561	0.00
N_2	-108.9803	-108.6923	-109.8645	-109.8581	-109.9087	-1.38
C_2H_2	-76.8431	-76.6250	-77.6106	-77.6077	-77.6402	-0.88
CO	-112.7756	-112.4706	-113.6548	-113.6503	-113.6997	-1.34
HCN	-92.9016	-92.6541	-93.7304	-93.7244	-93.7662	-1.14
CH_4	-40.2103	-40.1187	-40.7021	-40.7003	-40.7014	-0.03
C_2H_6	-79.2537	-79.0720	-80.1912	-80.1878	-80.1900	-0.06
NH_3	-56.2173	-56.1067	-56.7742	-56.7729	-56.7779	-0.14
LiF	-106.9827	-106.7022	-107.7350	-107.7340	-107.7796	-1.24
HCl	-460.0940	-459.3330	-461.7452	-461.7451	-461.8655	-2.61

Table 4: *Total energies (in Ha) of molecules in Hartree-Fock (HF), LSDA, rFLOSIC(g), rFLOSIC, and cFLOSIC and the total energy difference ΔE = cFLOSIC – rFLOSIC (in eV). The cFLOSIC energies are evaluated using the self-consistent rFLOSIC electron density. rFLOSIC(g) corresponds to energies relaxed with FLOSIC while rFLOSIC corresponds to LSDA equilibrium geometries. rFLOSIC and cFLOSIC results, at LSDA geometries, are from Ref. [25].*

3.4 Molecules

For completeness HF, LSDA, rFLOSIC, and cFLOSIC total energies calculated for selected molecules, taken from Ref. [25], are shown in Table 4 in Ha units. The energy difference cFLOSIC – rFLOSIC is shown in the last column in eV. The rFLOSIC total energy is considerably lower than the LSDA energy for each molecule in the table and the cFLOSIC energy is lower than rFLOSIC in all cases except Li_2. The complex/real energy difference depends on the nature of the molecule. For molecules involving only C−H or N−H bonds the differences are less than 0.15 eV . The differences are much larger for molecules with multiple bonds (C=C, C≡N, C=O, N≡N, O=O). For example in N_2, which has a triple bond, the cFLOSIC energy is 1.4 eV lower than for rFLOSIC. For O=C=O, with two double bonds, the energy difference is 2.8 eV. The largest energy difference is obtained for HCl, where the cFLOSIC energy is 2.61 eV lower than the rFLOSIC energy. Cl is the heaviest atom appearing in our set of molecules and the cFLOSIC energy of the isolated Cl atom is 3.34 eV lower than for rFLOSIC.

Atomization energies were calculated as the difference in the total energies of the molecules (Table 4). The results (in eV) for LSDA, rFLOSIC, and cFLOSIC are shown in Table 5, along with reference experimental values from which zero-point energies have been removed in order to be directly comparable to the computed values. The cFLOSIC atomization energies are sometimes larger and sometimes smaller than in rFLOSIC, but mostly larger than the LSDA values. Exceptions where the cFLOSIC atomization energies are smaller than in LSDA are for F_2 and O_3. Compared to the reference atomization energies, the FLOSIC methods have significantly smaller mean errors (MEs) than LSDA. The ME for LSDA, rFLOSIC, and cFLOSIC are 1.92, 0.63, and 0.85. rFLOSIC and cFLOSIC also have smaller mean absolute errors (MAE) than LSDA. The MAE for cFLOSIC (1.21 eV) is somewhat worse than for rFLOSIC (1.08 eV).

Molecule	Ref.	LSDA (eV)	rFLOSIC (eV)	cFLOSIC (eV)	ΔE (eV)
Li_2	1.05	1.01	1.03	1.03	0.00
CH_3	13.27	14.69	14.62	14.65	0.03
CH_4	18.21	20.03	20.26	20.21	-0.05
C_2H_6	30.83	34.40	34.72	34.62	-0.10
NH_3	12.88	14.60	14.49	14.16	-0.39
LiF	6.03	6.80	5.70	6.18	0.48
F_2	1.65	3.42	1.70	0.92	-0.78
HCl	4.64	5.26	5.09	5.02	-0.07
C_2H_2	17.52	19.90	18.92	19.65	0.73
HCN	13.57	15.59	14.35	14.95	0.60
CO	11.32	12.95	11.14	11.80	0.66
CO_2	17.00	20.46	16.11	17.58	1.47
N_2	9.84	11.53	10.25	10.70	0.45
O_3	6.42	10.47	4.73	4.71	-0.02
ME		1.92	0.63	0.85	
MAE		1.92	1.08	1.21	

Table 5: *Atomization energy (in eV) of molecules in LSDA, rFLOSIC, and cFLOSIC, and difference ΔE = cFLOSIC – rFLOSIC. The reference atomization energies are zero-point energy corrected experimental values. Mean error (ME) and mean absolute error (MAE) for each method relative to the reference are also shown. The cFLOSIC values were obtained from calculations using the self-consistent rFLOSIC density. Calculations performed by K. Withanage.*

It is instructive to compare LiF and HCl which both have an outermost valence of 8 paired FODs that form a distorted tetrahedron. For LiF, small energy differences (0.0025 in the case of LiF) occur depending on whether the base or the vertex of the tetrahedron is found between the two atoms. For LiF there are three nearest FODs to the Li atom. For HCl the tetrahedron is inverted and there is only one FOD in close proximity to the hydrogen atom. This distinction is due to changes in the energy splitting between the occupied s and unoccupied p states on the column-1 element.

3.5 Returning to N_2: complex vs. real FLOs

Pictured in Fig. 3 are isosurface plots of the valence orbital densities for N_2. The figure includes the canonical orbitals (top), the rFLOs (left) and the cFLOs (right) from real and complex FLOSIC calculations, respectively. The figure displays the SIC energy $E^{SIC}[n_{i\sigma}]$ for each orbital, as well as the expansion of the rFLOs and cFLOs in terms of the canonical orbitals. (Note that the definition of the canonical orbitals varies slightly between the rFLOSIC and cFLOSIC calculations. Primes are used to indicate this difference.) The centroids of the rFLOs and cFLOs are also shown in the figure. For the rFLOs, the centroids are close to the FOD positions. The canonical $2\sigma_u$, $1\pi_{ux}, 1\pi_{uy}$ and $3\sigma_g$ orbitals shown in Fig. 3 have positive SIC energy. The SIC energies are all negative for the rFLOs and cFLOs. The centroids of the rFLOs associated with the triple bond are positioned at the vertices of an equilateral triangle in a plane perpendicular to the bond axis and passing through its midpoint. This is indicated in the gray inset on the left

side of Fig. 3. For the rFLOSIC case, the centroids are close to the optimized FOD positions. The topology of the triple-bond rFLOs is similar to that of the localized orbitals discussed by Ruedenberg and Edmiston and also by Klüpfel *et al*. The optimal cFLOs on the right of the figure appear very similar to the complex local orbitals shown by Klüpfel *et al*. The FLOs corresponding to the lone pairs in N_2 are similar in the rFLOSIC and cFLOSIC calculations, although the cFLOs are slightly more localized.

The SIC energies shown in the figure indicate that the cFLOSIC total energy is lower than the rFLOSIC total energy due to the SIC energies of the triple-bond orbitals. Interestingly, one cFLO has a less negative SIC energy than any of the three equivalent rFLOs, but this is compensated by a much larger difference for the other two orbitals that have a more negative correction than the rFLOs. The cFLO optimization thus accepts an energy penalty for one orbital in order to realize a larger energy reduction for the other two.

It is interesting to examine the unitary transformation connecting the rFLOs and cFLOs to the canonical orbitals. This is shown in Fig. 3. The entries indicate that the three-triple bond rFLOs are symmetry-related mixtures of the $2\sigma_g$ and π_x and π_y canonical orbitals, essentially equivalent to bonding combinations of sp^2 hybrids. For the cFLOs, one triple bond orbital is a complex combination of the π_x and π_y orbitals yielding a cylindrical density. The other two are σ-π hybrids resulting from a complex π orbital and a real $2\sigma_g$ orbital. To the best of our knowledge, these simple expressions detailing the cFLOs have not been published previously. The two lone pair orbitals have complex coefficients that essentially correspond to a real number times the same complex phase factor for all three. Thus, these orbitals can effectively be taken as real, showing that the cFLOSIC optimization may result in real orbitals, when these minimize the energy. The centroids of the cFLOs are also shown in the panel on the right of Fig. 3. For the triple bond orbitals, these fall on a line passing through the bond center perpendicular to the axis. It is worth noting that the centroid of the cylindrical orbital is at the bond center where the π orbitals have zero amplitude. The Fermi orbital corresponding to a real FOD placed at the center of the bond would therefore contain zero contribution from the π orbitals. This is a reminder that orbital centroids do not always coincide with FOD positions.

To summarize, a scheme to introduce complex local orbitals (cFLOs) into the Fermi-Löwdin orbital self-interaction correction (FLOSIC) method has been derived and tested.. The scheme rests on allowing the Fermi orbital descriptors (FODs) to be complex. FOD optimization is accomplished via gradient optimization as in the case of FLOSIC restricted to real orbitals (rFLOSIC) and requires only the additional calculation of energy gradients with respect to the imaginary part of the FODs. We demonstrated the complex FLOSIC (cFLOSIC) method through applications to an array of atoms and molecules. The results of these applications are similar to those obtained in complex PZSIC calculations. The cFLOSIC solutions are generally lower in energy than in rFLOSIC. We showed that the optimal cFLOs are less localized than the analogous rFLOs, as judged by having a less negative self-Hartree energy. The lower cFLOSIC total energies thus arise from reducing the magnitude of the self-exchange-correlation energy of the cFLOs relative to the rFLOs. Analyzed in terms of individual orbital corrections, we find that the cFLOs lower the energy more for strongly hybridized orbitals and, in molecules,

for double and triple bond orbitals. The cFLOSIC calculations reported here make use of the self-consistent occupied orbitals from corresponding rFLOSIC calculations. A next step will be to make the cFLOSIC calculations fully self-consistent. Self-consistent cFLOSIC calculations will result in somewhat lower total energies that those presented in this section, but we do not expect significant changes to any of our conclusions. It is also of interest to perform cFLOSIC calculations with more sophisticated functionals such as PBE and SCAN. Finally, the results presented in this section indicate that SIC calculations on molecules with multiple bonds or transition metal atoms may be particularly affected by the use of complex orbitals.

4 Downward quantum learning: Tricks for finding starting configurations

We now discuss a search method which we refer to as downward quantum learning. As discussed above, finding initial FODs that lead to a positive definite Fermi orbital overlap matrix, a necessity for obtaining FLOs, is difficult especially for f-electron systems and open-shell systems regardless of whether they are isolated or in molecules or solids. For systems where charge-transfer exists between a cation and an anion, the Kohn-Sham orbitals obtained from a starting calculation are generally inadequate for starting a calculation. The systems just mentioned are of course the systems for which self-interaction corrections are most needed. In an earlier section an existence proof was provided. Let us now think about the manifestations of this proof.

Existence of FLOs for the free-electron metallic state

It is generally not known how to find FODs and FLOs for metals. It is however known that Wannier functions for a metallic state do not exist and this is why Wannier functions are in fact a subset of FLOs. While there has not yet been a demonstration for an exact set of FLOs for the metallic Brillouin zone, or Fermi-sphere, of the free-electron gas, we argue here that one exists. Wannier's demonstration in 1937 showed Wannier functions exist for a cubic (insulating) Brillouin zone and this chapter as well as earlier works by the author showed here these functions coincide with FLOs. Therefore, there is now hope, in fact a guarantee, for a semi-analytic solution of this problem. Once can start by inscribing a Fermi Sphere inside a Wannier Cube and then successively remove one FOD and one FLO, from outside the sphere, and inside the cube until only the Fermi Sphere remains.

Existence of FLOs for all Atoms

With respect to atoms it is generally quite easy to find starting positions for any rare-earth atom and more generally for any atom/ion that has closed-shell spin states and a qualitatively correct shell filling. The theorem proved above stated that for each of these "easy" solutions, one can determine initial FODs for lighter atoms by removing one orbital and one FOD because at least one $N-1$ dimensional cofactor has to be non-zero if the N-particle determinant is non zero.

This means that by mining the quantum information contained within the resulting FLOs for the heaviest rare-earth atom (Z=118, Oganesson) it is possible to obtain starting configurations for every atom in the problem. In the following we demonstrate this capability. A recent demonstration of principle is repeated here.

The existence proof reiterated above shows that viable FOD positions and complementary Kohn-Sham orbitals do indeed exist if the many-electron wavefunction does not vanish everywhere. This solution is especially useful for open-shell atoms and ions from the d- and f-blocks of the periodic table.

Nomenclature for FLO issues

To improve the nomenclature used for discussing the FLOSIC results and formulation, we outline five technical problems that arise. Three of these inconveniences are unique to FLOSIC while the others are also present in standard DFT calculations. However, these issues have both positive and negative attributes. Their presence often hampers a calculation technically when the user is only interested in the ground state. However they also provide physical insights for cases where energy- or electron-transfer is of interest. We refer to these issues as Fermi-Orbital-Challenges (FOCs). First, the ability to start calculations by finding an initial set of FODs and a Kohn-Sham density matrix that leads to a positive definite FO-overlap matrix must be fully systematized (FOC1). FOC1 arises for all cases where density-functional algorithms give qualitatively incorrect shell fillings – a problem that is prevalent in atoms containing $3d$/$4s$ states and $4f$/$5d$ states. FOC2 is exemplified by systems that have multiple low-lying competing electronic configurations which, depending on whether one is thinking in terms of DFT or WF, are either Janak-like multi-reference systems respectively. For such systems there are generally non-integer occupation numbers associated with the Kohn-Sham orbitals that oscillate from iteration to iteration. For standard DFAs, this leads to poor convergence in systems as simple as the Nickel atom or Carbon dimer and results that are not easy to interpret. Within FLOSIC, rather than finding a single fractionally occupied solution, multiple low-energy stable solutions with integer occupancy are determined. This feature readily provides the correct pictures for problems such as charge transfer. When multiple solutions exist there are generally incompatibilities between the FODs for one solution, and Kohn-Sham orbitals for other solutions. These incompatibilities complicate the determination of starting solutions. While FOC2 is a significant frustration to users, it also identifies systems that may have interesting low-energy excitations which is generally relevant in energy applications. FOC3 presents the user with multiple stable states that are sometimes incorrectly associated with incorrect ground states but most likely contain information about collective excitations such as plasmon oscillation. Other *aufbau*-violating solutions associated with FOC3 may provide information about x-ray excitations. A spin-conserving example of FOC3 is charge transfer excitations between a halide and alkali in the stretched bond limit (NaCl $\rightarrow$ $Na^{+1}Cl^{-1}$) or the charge transfer excitations in light-harvesting systems. The latter are *aufbau* violating solutions at the DFT-level but may be *aufbau* consistent solutions within FLOSIC. FOC3 is always a clear indicator of mul-

tiple low-energy excitations or multi-reference character. It is a frustration when the primary interest is on the ground state but is advantageous when one is interested in studying molecular processes especially those related to luminescence and fluorescence in, for example, rare earths.

FOC4 and FOC5 are related to symmetry breaking in the density-functional formulation. It is generally accepted that the description of stretched bonds or dissociated atoms, within density-functional pictures, requires spin symmetry breaking with excess spin-up density on one atom and excess spin-down density congregating on an otherwise symmetrically equivalent atom. Such antiferromagnetic pictures lead to total densities that do not break the overall symmetry of the molecular system. Analogous symmetry breaking occurs within systems that are treated with FLOSIC (FOC4). Further when a partial open-shell structure occurs (ozone is a deceptively simple case), FLOSIC predicts spin separation but standard functionals do not. The conundrums presented by FOC4 and FOC5 are similar but one is driven by the self-interaction correction rather than the energy functional it self. As such we label FOC4 and FOC5 as separate challenges. Issues arising from FOC3–FOC5 raise the spectre for better descriptions of low-energy spin-conserving (FOC3) and spin-changing (FOC4–FOC5) excited states. The count-down paradigm discussed below is based on the rigorous existence proof presented above and provides a new tool for constructing self-consistent *aufbau*-violating states for systems where occupation number constraints might fail. The procedure does not circumvent FOC2 issues. Such issues will continue to require improvements on the iterative process and/or additional attention to occupation-number dependent FLOSIC formulations.

Generally speaking, closed shell atoms are the simplest cases for finding viable starting FODs. Yet even in those cases locating useful FOD starting points can be difficult. To give an indication of the challenge, we share our experiences for finding FODs in Radon (Z=86), We used a Monte Carlo approach to generate many sets of FOD positions for individual shells corresponding to the various principal quantum numbers n of the occupied orbitals. Each shell had a radius equal to the average radial expectation value of the corresponding orbitals. A total of n^2 positions were randomly placed on each shell (a spin unpolarized atom was assumed). This approach resulted in viable FODs in fewer than 8 percent of the trials. For other heavy atoms, especially those between La and Hg, the success rate was even lower. Using a solution for Rn, removing FODs, and starting from default atomic density-functional potentials, allowed successful calculations for a small number of atoms (Eu, Yb, Au–Rn). This success, while limited, highlighted the need for the solution discussed below.

Here we present a well-defined way to determine initial FOD positions to start a calculation. The method is based on a proof given below that a set of viable FOD positions has the property that a Slater determinant of the KS orbitals is non-zero when evaluated at the FOD positions. The ability to extract FLOs and FODs from clearly closed-shell systems and then systematically investigate on-atom Kossel-like solutions in the actinides and lanthanides is an additional need that the method described here addresses. For the calculations reported here, we used a legacy version of the NRLMOL software package that utilizes optimized cartesian gaussian basis sets and a highly accurate numerical integration scheme. The version employed was developed approximately 20 years ago to assess the possibility that scalar relativity could significantly

impact second-order anisotropy energies in $4d$ molecular magnets. The possibility of using f-electrons for post-processing of anisotropy Hamiltonians was incorporated at that time and basis sets for nuclear charges between Ba–Rn were generated using the techniques. Shortly after the MMQT group formed at UTEP in 2019, methods for performing self-consistent-field calculations with f-electrons were completed. These methods used integral transforms, albeit for gaussians. The Fermi-Löwdin methodology was simultaneously inserted into the legacy f-electron code. However in contrast to the earlier versions of the FLOSIC code, the formulation was implemented in a manner that preserved the group-theoretical methods that are part of the legacy NRLMOL codes. We viewed this as a necessary addition from the standpoint of efficiently finding FODs for heavy open-shell atoms. Group-theoretical techniques simplify the optimization of the basis sets for elements between Rn and Og (Z=86–118).

4.1 Initializing FODs for principal quantum numbers with *n*=2, 3, and 4

In the motivation we asked if there are lattices that are reciprocal to an arbitrary set of Kohn-Sham orbitals. For finite systems, we refer to these lattices, or polyhedra, as flotonic solids. We have used the T_d group operations to search for a set of equi-radial FODs with T_d symmetry that lead to a set of 16 points on the unit sphere with a large determinant. T_d symmetry allows for equivalent shells of 1, 4, 6, 12, and 24 points, respectively. To find a set of 16 points we have followed the prescription of placing 12 points on the unit sphere and found that, in addition to the dodecahedron there are many sets of 12-site shells that are compatible with T_d symmetry for which the 12×12 matrix constructed from l=2 and l=3 spherical harmonics leads to non-singular matrices. We listed approximately 20 of these solutions and then combined them with the 4-site T_d shells to create a family of 16-site FODs. We then re-ordered the family of 16-site solutions according to the determinant of the 16×16 $\underline{\mathrm{W}}$-matrix and found that there are two solutions with anomalously large determinants. The solution with second largest determinant turned out to be the best solution for the radon atom, strengthening the hypothesis that one should use spherical harmonics to find universal sets of FODs. It appears that a key figure of merit of a point group is that it must not contain the inversion operator since the presence of inversion prevents mixing of states with opposite parity. The octahedral point group, O_h, has two subgroups of order 16 which might provide additional solutions for the n=4 shells, but so far we have not found such solutions. As known from the periodic-table and represented in Table 6, noble-gas atoms correspond to atoms that contain subsets of electronic states that share a principal quantum number and have a similar atomic radius. For each principal quantum number n, there are n^2 hydrogenic-like orbitals with $n^2 = \sum_{l=0}^{n-1}(2l+1)$.

We then can consider the lowest n^2 spherical harmonics on a unit sphere. Depending on the value of n this yields a sequence of matrices of dimension $n^2 = \sum_{l=0}^{n-1}(2l+1)$, or 1, 4, 9, and 16 for n=1, 2, 3, and 4, respectively. For each of these cases a $\underline{\mathrm{W}}$-matrix can be constructed

according to

$$\underline{\mathrm{W}} = \begin{bmatrix} Y_{00}(\hat{a}_1) & Y_{1,-1}(\hat{a}_1) & Y_{1,0}(\hat{a}_1) & Y_{1,1}(\hat{a}_1) & \cdots & Y_{n-1,-n+1}(\hat{a}_1) & \cdots & Y_{n-1,n-1}(\hat{a}_1) \\ Y_{00}(\hat{a}_2) & Y_{1,-1}(\hat{a}_2) & Y_{1,0}(\hat{a}_2) & Y_{1,1}(\hat{a}_2) & \cdots & Y_{n-1,-n+1}(\hat{a}_2) & \cdots & Y_{n-1,n-1}(\hat{a}_2) \\ \vdots & \vdots & \vdots & \vdots & \cdots & \vdots & \cdots & \vdots \\ Y_{00}(\hat{a}_{n^2}) & Y_{1,-1}(\hat{a}_{n^2}) & Y_{1,0}(\hat{a}_{n^2}) & Y_{1,1}(\hat{a}_1) & \cdots & Y_{n-1,-n+1}(\hat{a}_{n^2}) & \cdots & Y_{n-1,n-1}(\hat{a}_{n^2}) \end{bmatrix}_{n^2 \times n^2} \quad (48)$$

The goal then is to pick sets of n^2 points on a unit sphere that, at the very minimum, guarantee that no spherical harmonic with angular momentum less than or equal to $n-1$ vanishes at all points but with the stricter and more difficult condition that the above matrix is non-singular. A systematic and fast way to find sets of points is to generate all sets of points on a cubic grid (n_x, n_y, n_z) with $|n_x| < 7$ (higher numbers do not change the outcome), and then normalize them onto a unit sphere. One can then search over all point groups to find high-symmetry arrangements of 4, 9, or 16 points. These can then be used to evaluate the determinant of $\underline{\mathrm{W}}$ in Eq. (48). The sets corresponding to the largest determinants then suggest the best sets of FODs for electrons sharing the same principal quantum number. The effect of these sets on the determinant of the FOD overlap matrix is shown in Table 7. The best 9-electron set located so far, consisting of staggered triangles, gives sp^3d^5 hybrids and probably limits the symmetry of the overall atomic spin density to C_{3v}. The optimal shells obtained for element 118 (Og) are presented and we show how these shells can be used to generate starting points for all other noble-gas atoms. The tetrahedral (T_d) shells, which describe sp^3 (n=2, n^2=4) systems have been well understood for quite some time. However, the sp^3d^5 (n=3, n^2=9) and $sp^3d^5f^7$ (n=4, n^2=16) shells are significantly more difficult to determine as random guesses and are deserving of additional discussion.

As a representative example, we describe the series of calculations beginning with the self-consistent closed-shell calculation for Ar (Z=18) that features filled $3s$ and $3p$ sub-shells for the outer electrons, in addition to completely filled n=1 and n=2 shells. For a shell with 4 electrons, FODs can be arranged at the vertices of a tetrahedron. The resulting FLOs are sp^3 hybrid orbitals. We adopt radii of 1.73 and 0.45 Bohr for the n=2 and n=3 tetrahedrons, respectively. We then computed the total energy self-consistently with the LSDA density functional, obtaining a PZSIC total energy of -529.9441 Ha, and an orbital energy for the highest occupied molecular orbital (HOMO) of -0.6141 Ha, corresponding to a predicted removal energy (the negative of the HOMO energy) of 16.7 eV. The corresponding value in an uncorrected LSDA calculation is 10.4 eV. The experimental ionization potential (IP) for Ar is 15.8 eV. These results reflect the well-known effect of self-interaction in atoms that the HOMO eigenvalues are smaller than ionization energies. Calculated LSDA and FLOSIC removal energies and corresponding experimental IPs are shown in Table 8.

From the self-consistent Ar calculation, one of the outermost FODs and one of the occupied Kohn-Sham orbitals are removed in order to create starting FLOs for a FLOSIC calculation for Cl. Similarly, two outer FODs and two KS orbitals are removed (of the same spin) to create a starting point for a FLOSIC calculation for S. This process was repeated for all the atoms of the second row. Predicted removal energies obtained from the calculations can be found in

Config.	$\vec{A}$	Sym.	N_{equiv}	R_{Og}	R_{Rn}	R_{Xe}	R_{Kr}	R_{Ar}	R_{Ne}	R_{He}
s	$(0,0,0)$	N/A	1	0.0000	0.000	0.00	0.00	0.00	0.00	0.00
sp	$\vec{A}_1$	T_d	4	0.0356	0.074	0.12	0.19	0.44		
spd	$\vec{A}_2^1$	T_d	6	0.1012	0.18	0.33				
spd	$\vec{A}_2^2$	C_{3V}	3	0.1012	0.18	0.33				
$spdf(A)$	$\vec{A}_3^1$	T_d	4	0.2808	0.43					
$spdf(B)$	$\vec{A}_3^2$	T_d	12	0.2808	0.43					
$spdf$	$-\vec{A}_3^1$	T_d	12	0.6138						
$spdf$	$-\vec{A}_3^2$	T_d	4	0.6138						
$spd(C)$	$-\vec{A}_2^1$	T_d	6	0.9045	1.00	0.85	0.60			
$spd(D)$	$-\vec{A}_2^2$	C_{3V}	3	0.9045	1.00	0.85	0.60			
sp	$-\vec{A}_1$	T_d	4	2.4656	2.47	2.28	1.92	1.68	1.07	

Table 6: *Reasonable starting FODs and radii for noble gas atoms. Symmetrized sets of unit-vectors that maximize the $n^2 \times n^2$ determinant of spherical harmonics on a unit sphere are given by: $\vec{A}_1 = (1,1,1)/\sqrt{3}$, $\vec{A}_2^2 = (1,0,0)$ and $\vec{A}_2^2 = (-1,-1,2)/\sqrt{6}$, $\vec{A}_3^1 = (1,1,1)/\sqrt{3}$ and $\vec{A}_3^2 = (-0.8789,-0,3373,-0.3373)$. Based on Linnett-like structures for inverting FOD-positions for opposite spins, the highest symmetry for the spin-densities in Ne and Ar is T_d while the symmetry of the density can be O_h. Similarly the highest symmetry for the spin-density for Kr–Og is C_{3v} while the symmetry for the total density can be D_{3d}. A variety of lower point group symmetries that would be compatible with incomplete shells of angular momenta are possible in other ions. The flotonic solids that result from these vectors and the resulting n^2 hybrids (for n=3 and 4) are illustrated in Fig. 2. While the shells for each principal quantum number close to resolved, the relative orientation of each shell is not resolved at the time of this writing. Standard optimization methods are not good at addressing such questions and additional automation is required for perfecting that part of the FOD optimization.*

Table 8, where it can be seen that the FLOSIC predictions are much closer to the experimental values. Similar downward-quantum-learning calculations have been performed starting from Og (Z=118), Rn (Z=86) and Ne (Z=10) [27].

Here, we have provided an existence proof that connects viable FOD positions to a non-zero value for the many-electron wave function constructed from the Kohn-Sham orbitals for the system and evaluated at the FOD positions. The proof relies only on the properties of determinants and it guarantees that if one finds viable FODs for a system of N electrons, it is always possible to find viable FODs for electronic systems with fewer electrons (in each spin channel), using a countdown algorithm that selectively removes FODs and orbitals from the N-electron solution. For any set of orbitals unitarily equivalent to the KS orbitals, the algorithm identifies at least N solutions of lighter systems constructed by successive removal of orbital-FOD pairs. It is very possible that successive removal of FLO-FOD pairs will generate a total of $\sum_{n=1}^{N-1} \binom{N}{n} = 2^N - 2$ initial solutions for atoms containing between 1 and $N-1$ electrons of a specific spin. We demonstrated that the algorithm can successfully generate FODs for lighter

Z	$\det^{1/2}$	Z	$\det^{1/2}$	Z	$\det^{1/2}$	Z	$\det^{1/2}$	Z	$D^{1/2}$	Z	$D^{1/2}$
59	0.0003	58	0.0003	57	0.0004	56	0.0004	55	0.0004	54	0.0008
53	0.0016	52	0.0033	51	0.0044	50	0.0059	49	0.0077	48	0.0101
47	0.0133	46	0.0171	45	0.0190	44	0.0210	43	0.0225	42	0.0241
41	0.0265	40	0.0284	39	0.0294	38	0.0333	37	0.0363	36	0.0377
35	0.0391	34	0.0403	33	0.0416	32	0.0426	31	0.0438	30	0.0453
29	0.0523	28	0.0600	27	0.0667	26	0.0740	25	0.0846	24	0.0967
23	0.1065	22	0.1298	21	0.1518	20	0.1606	19	0.1753	18	0.1943
17	0.2109	16	0.2289	15	0.2433	14	0.2638	13	0.3861	12	0.5644
11	0.8240	10	0.8683	9	0.9111	8	0.9456	7	0.9702	6	0.9870
5	0.9901	4	0.9943	3	0.9974	2	0.9993	1	1.0000		

Table 7: *Determinant ($\det^{1/2}$) of the Fermi-orbital overlap matrix for electronic configurations of Og^{+Q}. The fact that the determinant for every electronic configuration converges monotonically from the determinant of the neutral Og atom to 1 guarantees that it is possible to generate relatively physical starting points for any charge and spin state of any atom.*

atoms from a solution for the next-largest noble gas atom. This has been accomplished for all atoms below Ne and Ar, and for select atoms beginning from solutions for Rn and Og (Z=86) and Og (Z=118). The success of the algorithm across the periodic table demonstrates its utility and numerically confirms the theorem repeated above and first demonstrated in Ref. [27]. For atoms in d- and f-blocks of the periodic table, additional integration of existing and additional techniques are progressing. These techniques include: (1) single-shot Z-dependent scaling of the starting orbitals using a combination of the data in Table 1 and 6, and shell-by-shell virial-like scaling, (2) optimization of FODs at the frozen density, (3) facile but more sophisticated potential biasing of starting potentials that are discussed in Ref. [22] and [25], (4) new machine-learning strategies that aid predicting which of the $2N$ solutions identified from the countdown method are most likely to succeed, and (5) capitalizing on the ligand-induced changes in atom coordination that ultimately define the allowable $3d$ and $4f$ valence configurations in atoms. We expect that complete success in generating self-consistent solutions using the countdown algorithm will require scaling the starting orbitals obtained for the heavier atoms. Because of the larger Z, the wave functions of the closed-shell atoms are too compact for the lighter atoms. This can cause problems during the self-consistent iteration process that cause the calculation for the lighter atom to fail. An alternative approach will be to reduce the value of the nuclear charge of the lighter in several steps from that of the closed-shell atoms to its correct value, while generating self-consistent wave functions at each steps. The algorithm can be used to find a variety of solutions for lighter atoms, corresponding to various occupations of the orbitals. This means that the method could be used to generate a database of starting FODs for atoms throughout the periodic table, in various charge states and oxidation states, beginning from a solution for element Og, Z=118. With such a database automated starting points of viable FOD positions could also be created for molecules and other condensed systems.

The method proposed here succeeded by considering sets of 4, 9, or 16 points created by symmetry equivalent normalized vectors and was then used for the common special cases for par-

Atom	LDA	FLOSIC	EXPT.	Atom	LDA	FLOSIC	EXPT.
Ar	10.38	16.71	15.76	Ne	13.54	24.35	21.56
Cl	8.30	14.16	12.97	F	10.34	20.20	17.42
S	6.24	11.91	10.36	O	7.40	16.39	13.62
P	6.34	10.95	10.49	N	8.39	15.76	14.53
Si	4.65	8.89	8.15	C	6.11	12.46	11.26
Al	3.05	6.98	5.98	B	4.10	9.36	8.30
Mg	4.78	8.49	7.65	Be	5.59	10.84	9.32
Na	3.11	6.46	5.14	Li	3.17	6.92	5.39
Rn	7.98	11.90	10.75	Og	7.44	11.20	8.9
At	6.68	10.52	9.22	Ts	5.99	9.89	7.70
Po	5.35	9.19	8.42	Lv	4.95	8.67	8.64
Bi	5.40	8.70	7.29	Mc	5.11	8.42	5.68
Pb	4.18	7.35	7.42	Fl	3.96	7.25	8.53
Tl	2.96	6.10	6.11	Nh	2.83	6.07	7.31

Table 8: *Calculated (-1)HOMO energies from DFT-LDA and FLOSIC, and experimental ionization energies of atoms (in eV). Ionization energies for the superheavies may be found on the web. Some of the early experimental results are inconsistent with our FLOSIC results and trends expected from the Rn row.*

tially filled electronic shells. It points further to an improved method for rapid characterization of other solutions. If we loop over point groups, one can then create sets of equivalent points that are compatible with that point group. Given a set of Q points one can ask whether there are exactly Q combinations of the first 16 spherical harmonics that are linearly dependent on the unit sphere. When this condition holds FOC1 has been bypassed for a specific partially filled shell of angular momenta sharing the same principal quantum number. A further improvement for this case would be to hypothesize that the local coordinate system should be oriented such that some of the Q points coincide exactly with the zeros of the missing spherical harmonics. This point is expected to be particularly useful for molecular magnets for which local Jahn-Teller distortions, defined by the ligand structures, mandate shell fillings with holes in the frontier d- or f-shells.

4.2 Challenge: Simulating tetra-anionic Mn_{12}-Acetate in water

Learning how to control solar-induced splitting of water into oxygen and hydrogen would have immense value from the standpoint of the world energy and climate concerns. For computational materials scientists and physicists to help with this problem there are many multi-scale problems that need to be solved and quantum-mechanical methods for understanding these problems will require scientists to accurately simulate highly charged molecular systems in aqueous environments. Typical problems that occur when simulating a single ion near water is that fractionally occupied states occur at the Fermi level with the excess electron spread over the solvent (water) and the solute (anion). In Table 9 we show energy differences, calculated within PBE-GGA, for a chemical system containing four excess electrons. In going from S_0

State	Molecular Configuration	Energy (eV/H2O)
S_0	$Mn_{12}O_{12}(COOH)_{16}(H_2O)_4$ + $4H_2O$ + 4e-	0.00
S_1	$Mn_{12}O_{12}(COOH)_{16}(OH^-)_4$ + $4H_2O$ +$2H_2$	0.95
S_2	$Mn_{12}O_{12}(COOH)_{16}(H_2O)_4$ + $4(OH^-)$ +$2H_2$	1.34
S_3	$Mn_{12}O_{12}(COOH)_{16}(H_2O)_4^{4-}$ + 4(OH) +$2H_2$	2.62
S_4	$Mn_{12}O_{12}(COOH)_{16}(H_2O)_4$ + $4H_2O$ + 4e-	0.00

Table 9: *A cyclic catalytic water-splitting reaction sequence. The energy scale for various tetra-anion configurations are somewhat consistent with the experimental observation that four electrons are needed to split water. Full scale simulation on this type of problem requires corrections to the LUMO levels of solvated anions in water. Recent work suggests that FLOSIC will correct for such issues. [23]*

to S_1, terminating water molecules expel neutral hydrogens which then form molecular hydrogen leaving behind the isoelectronic hydroxyl anions in place of the waters. In going from S_1 to S_2, waters of solvation replace the hydroxyl anions which returns the molecule to its initial state. In the following two steps the electrons are transferred back to the molecule and the neutral hydroxyl radicals could convert into additional molecular oxygen and hydrogen. This is a straw-man hydrogen production cycle which may or many not hold water when put to rigorous computational testing. But the problem with computationally testing this hypothesis is, due to the self-interaction error, the HOMO level of the tetra-anion is predicted to be 6 eV above the LUMO of the surrounding molecule. FLOSIC calculations performed on the fragments suggest that inclusion of SIC for the entire system would place the tetra-anionic HOMO level very close to the LUMO level of the surrounding water molecules. Such conditions would be ideal for solar-induced hydrogen production. Problems such as this and other problems associated with highly charged anions in solution are one of many fertile areas for exploration with FLOSIC over the coming years. Additional discussion of this problem may be found in Ref. [23].

5 Summary and outlook

Including self-interaction corrections to density functional approximations (SIC-DFA) has been a long-standing challenge especially from the standpoint of maintaining the inherent efficiency of DFA methods in applications to molecular systems and devices. Early applications of SIC-DFA, based upon solutions of the localization equations [9, 11], succeeded in addressing the lack of unitary invariance in SIC-DFA and introduced a Koopmans' theorem [11]. We have reviewed a new implementation of the self-interaction-correction [19], now referred to as Fermi-Löwdin-Orbital Self-Interaction Correction (FLOSIC), that restores much of the formal structure expected from a DFA. Use of the density matrix, constructed from Kohn-Sham orbitals, and a physically appealing classical electron geometry, determines a density-dependent $N\times N$ unitary transformation that connects the occupied Kohn-Sham orbitals to the ideal localized orbitals for evaluation of the self-interaction correction. In the small N limit the FLOSIC method is at least N times slower than DFA. However, at the time of this writing, recent progress that

capitalizes on the intrinsic sparsity of the problem significantly reduces the cost. A downward-counting algorithm and existence proof have demonstrated applicability to all atoms in the periodic table [27]. This paper also provided an interesting connection between the FLOs and the amplitude of a Slater determinant composed of Kohn-Sham orbitals and raised the possibility of stronger connections between density-functional and wave-function pictures. Together with a sparse implementation of FLOSIC, there is now the possibility that the cost of a FLOSIC calculation, relative to LDA/GGA/SCAN, will have the exact same scaling as DFT and be within a factor of 10 of the cost. For example a soon to be reported application to a tri-anion-water system, $Cr^{III}(C_2O_4)_3$:$(H_2O)_{117}$, reduced the overhead from a factor of 1300 to, at most, 30.
The discussion here on the Fermi-Löwdin formulation of the self-interaction correction has attempted to provide the reader with the knowledge needed to embark upon their own original investigations. While the author opines that self-interaction corrections might decrease the need for spin-density-gradients in functionals, this has definitely not been proven here nor elsewhere. Complete analysis still requires a significant focus on implementation and efficiency but there are good reasons to expect that, as the FLOSIC community grows, new algorithms for implementation will be invented and the number of applications amenable to inquiry within the FLOSIC formalism will grow. The use of the FLO formalism is not limited to SIC and one can imagine applying the formulation to other quantum theories where unitary invariance is lacking. What is clear at this time is that basis set quality is seldom the accuracy limiting step in electronic structure calculations and it is probably still not time for the community to seriously invest their time in considering uncertainties due to basis sets. I have also provided my perspective on the status of the FLOSIC formulation and have tried to avoid encumbering the reader with too much cross comparison to other methods. The reader interested in works by others is encouraged to perform literature searches for the researchers mentioned in the acknowledgements. Finally, readers that are inspired to apply FLOSIC to problems that they are interested in, are encouraged to visit `https://www.flosic.org` to download the latest version of the publicly available FLOSIC code. Within that distribution, or via email to this author, it will also be possible to obtain a portable version of the legacy code which has some learning modules attached to it.

Acknowledgements

In finishing this book chapter and with confidence that the best days for the Fermi-Löwdin orbital formalism are still in front of us, I am thankful to competitors and collaborators for sharing ideas, questions, programming skills, and their individual contributions. I thank Dr. Eva Pavarini and Dr. Erik Koch for the opportunity to provide a perspective on this area of density-functional theory that has captured my curiosity for decades. Thanks to Dr. Alex Zunger and Dr. John Perdew for formulating SIC just as I was leaving college and entering graduate school and for many interesting discussions along the way. Thanks to Dr. Chun C. Lin for assigning an interesting dissertation topic and Dr. Richard A Heaton for collaboration during graduate school and for first suggesting, in August 1986, that Luken's early insights might provide a solution to the self-interaction problem. Thanks to Adrienn Ruszinzsky and John Perdew for collab-

oration on the introduction of FLOSIC. To Dr. Tunna Baruah, Dr. Jens Kortus, Dr. Der-You Kao, Dr. Javaria Batool, Dr. Torsten Hahn, and Dr. Koblar A. Jackson, I express my profoundest gratitude for their continuing interest in what are now called Fermi-Löwdin orbitals and for enthusiastic early efforts. There are numerous researchers from the Naval Research Laboratory, Max-Planck-Institut für Festkörperforschung, Daresbury National Laboratory, Linnaeus University, Freiberg Institute of Technology, University of Iceland and the University of Texas at El Paso that I have had stimulating discussions with on this problem. I note important contributions – both technical, computational, and scientific – from Dr. D.V. Porezag, Dr. J. Peralta, Dr. Yoh Yamamoto, Dr. Zahra Hooshmand, Dr. Kushantha Withanage, and Dr. Rajendre Zope. And thank you for reading this. I hope you will find time to read many interesting and important papers by these authors. The later part of this work (post 2020) was supported by the CCS FLOSIC project under the U.S. Department of Energy, Office of Science, Office of Basic Energy Sciences, under award number DE-SC001833.

References

[1] L. Pauling, J. Am. Chem. Soc. **53** 1367 (1931)

[2] T. Koopmans, Physica **1** 104 (1934)

[3] G.H. Wannier, Phys. Rev. **52**, 191 (1937)

[4] P.-O. Löwdin, J. Chem. Phys. **18**, 365 (1950)

[5] C. Edmiston and K.Ruedenberg, Rev. Mod. Phys. **35**, 457 (1963)

[6] I. Lindgren, Int. J. Quantum Chem. Symp. **5**, 411 (1971)

[7] J.F. Janak, Phys. Rev. B **18**, 7165 (1978)

[8] J.P. Perdew and A. Zunger, Phys. Rev. B **23**, 5048 (1981)

[9] M.R. Pederson, R.A. Heaton and C.C. Lin, J. Chem. Phys. **80**, 1972 (1984)

[10] W.L. Luken and J.C. Culberson, Theo. Chim. Acta **66** 279 (1984)

[11] M.R. Pederson, R.A. Heaton, and C.C. Lin, J. Chem. Phys **8**2, 2688 (1985)

[12] M.R. Pederson and C.C. Lin, Phys. Rev. B **35**, 2273 (1987)

[13] M.R. Pederson and C.C. Lin, J. Chem. Phys. **88** 1807-1817 (1988)

[14] A. Svane and O. Gunnarsson Phys. Rev. Lett. **65**, 1148 (1990)

[15] O.A. Vydrov and G.E. Scuseria, J. Chem. Phys. **121**, 8187 (2004)

[16] A. Ruzsinszky, J.P. Perdew, G.I. Csonka, O.A. Vydrov, and G.E. Scuseria, J. Chem. Phys. **125**, 194112 (2006)

[17] Z. Szotek, W.M. Temmerman, D. Ködderitzsch, A. Svane, L. Petit, and H. Winter, Phys. Rev. B **74**, 174431 (2006)

[18] S. S. Klüpfel, P. Klüpfel, and H. Jónsson, Phys. Rev. A **84**, 050501 (2011)

[19] M.R. Pederson, A. Ruzsinszky, and J.P. Perdew, J. Chem. Phys. **140**, 121103 (2014)

[20] M.R. Pederson, J. Chem. Phys. **142**, 064112 (2015)

[21] M.R. Pederson and T. Baruah: *Self-Interaction Corrections Within the Fermi-Orbital-Based Formalism*, Adv. At. Mol. Opt. Phys. **64**, 153-180, ed. by E. Arimondo, C.C. Lin, and S.F. Yelin (Academic Press, 2015)

[22] D.-Y. Kao, K. Withanage, T. Hahn, J. Batool, J. Kortus, and K.A. Jackson, J. Chem. Phys. **147**, 164107 (2017)

[23] J. Batool, T.Hahn, and M.R. Pederson, J. Comput. Chem. **40** 2301 (2019)

[24] S. Akter, Y. Yamamoto, C.M. Diaz, K.A. Jackson, R.R. Zope, and T. Baruah, J. Chem. Phys. **153**, 164304 (2020)

[25] K.P.K. Withanage, K.A. Jackson, and M.R. Pederson, J. Chem. Phys. **156** 231103 (2022)

[26] J.I. Melo, M.R. Pederson, and J.E. Peralta, J. Phys. Chem. A **127**, 527 (2023)

[27] M.R. Pederson, A.I. Johnson, K.P.K. Withanage, S. Dolma, G.B. Flores, Z. Hooshmand, K. Khandal, P.O. Lasode, T. Baruah, and K.A. Jackson, J. Chem. Phys. **158** (2023)